Università degli Studi di Tor Vergata Roma
Facoltà di Ingegneria

Dipartimento di Informatica Sistemi e Produzione

Ph.D. Geoinformation Programme

Use of hyperspectral and multi-angle CHRIS Proba image for land cover maps generation

Tesi di Laurea di

Riccardo Duca

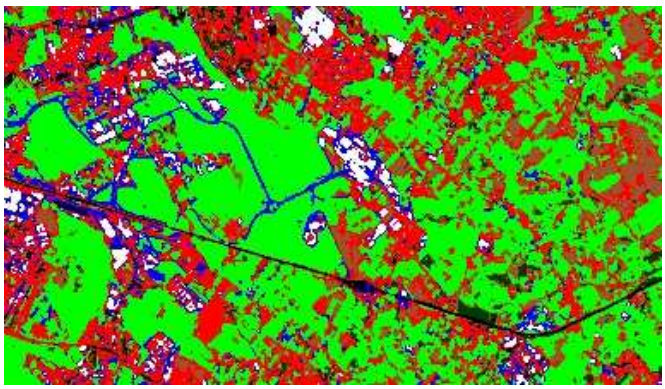

Relatore: Prof. Fabio Del Frate

Sessione di laurea Maggio 2008

Contents

List of Figures

List of Tables

List of acronymous

AATSR: **A**dvanced **A**long-**T**rack **S**canning **R**adiometer

ADEOS: **AD**vanced **E**arth **O**bservation **S**atellite

AERONET: **A**erosol **R**obotic **N**etwork

AMTIS: **A**irborne **M**ulti-angle **T**IR/VNIR **I**maging **S**ystem

AVHRR: **A**dvanced **V**ery **H**igh **R**esolution **R**adioneter

CHRIS: **C**ompact **H**igh **R**esolution **I**mages **S**pectrometer

CNR: Consiglio Nazionale delle Ricerche

DAISEX: **D**igital **AI**rborne **S**ectrometer **EX**periment

ESA: **E**uropean **S**pace **A**gency

ETM+: **E**nhanced **T**hematic **M**apper

FFT: **F**ast **F**ourier **T**ranform

FZA: **F**ly by **Z**enith **A**ngle

GCP: **G**round **C**ontrol **P**oint

GIS: **G**eographic **I**nformation **S**ystem

GLCF: **G**lobal **L**and **C**over **F**acility

HRC: **H**igh **R**esolution **C**amera

MERIS: **M**edium **R**esolution **I**maging **S**pectrometer

MISR: **M**ulti-angle **I**maging **S**pectro**R**adiometer

MODIS: **M**oderate **r**esolution **I**maging **S**pectroradiometer

MZA: **M**inimum **Z**enith Angle

POLDER: **POL**arization and **D**irectionality of the **E**arth's **R**eflectances

SPOT: **S**ystèm **P**our l'**O**bservation de la **T**erre

SWIR: **S**hort **W**ave **I**nfra **R**ed

TOA: **T**op **O**f **A**tmosphere

VHR: **V**ery **H**igh **R**esolution

Abstract

In the last decades, many satellite missions have marked the history of the optical remote sensing, providing a wide choice of products for every kind of application and investigation. The Proba-1 program can not be compared in importance and budget to the very important missions like Landsat and SPOT, but the innovations introduced in the payload design have attracted the attention of principal investigators and scientists since the beginning. The new spectral configuration of its high resolution sensor CHRIS can represent an innovation for the wide family of the optical instruments. In fact CHRIS is one of the first experiments, as well as NASA Hyperion, concerning the developing of the expensive hyperspectral technology for the satellite environment. Moreover, the innovative solutions for the autonomous orbit maintaining and navigation, permit to the spacecraft difficult manoeuvres and multi-angular acquisitions during the target overpass. The result is an extraordinary and unique database of hyperspectral and multi-directional images acquired several times during the years over predefined test sites.

This research work proposes a complete treatment of the CHRIS products since the radiometric and geometric correction till the classification processing. Phases like destriping, atmospheric corrections, spectral adjacency compensation and ortho-rectification have been performed and developed. Several classification exercises have been proposed with the aim of evaluating

the impact of the principal key factors of the Proba mission (hyperspectral, multi-angular and multi-temporal) to the final classification accuracy. The directional anisotropy of the reflectance, as well as its temporal dependence, has been well explained and investigated trough the use of spectral models and radiative equations, but studies and applications based on real satellite high resolution data over lands and water bodies are few or still ongoing. Said that, this research work has been addressed to asses if these additional information, which reflect additional costs in terms of satellite technology and image processing are justified with significant improvements for the land cover production, as one of the most diffused application in the research environment.

Once again the neural networks have confirmed their effectiveness for the classification of optical images at high and very high resolution. The new spectral, multi-angular and multi-temporal inputs have been well managed and used as additive information for the decision task, without impacting the design of the classification scheme. On the whole the results have been satisfactory in most cases.

Chapter 1

Introduction

1.1 From multi-spectral to hyper-spectral imagery: the evolution of the optical sensors

It's now about 35 years since the first multi-spectral Landsat sensor was launched. The Landsat family represented the first possibility for the production of land cover and vegetation index maps at high spatial resolution (around 20-30 meters) from satellite data. All the Landsat missions have represented for years the reference point for the scientific community involved into the processing and exploitation of the optical data, demonstrating that the multi-spectral high resolution technology represents one of the best solution for many scientific and commercial applications. For this reason this technology is still having notable improvements, exploring new spectral configurations joined with new capabilities in terms of revisit time and geometry of view. Although the Landsat-like multi-spectral images are still now widely used, the evolution of the optical sensors in different directions has been unavoidable and especially in the last two decades this evolution has produced

a wide choice of products for the users.

The first SPOT mission opened the epoch of very high resolution instruments, making available new images characterized by a reduced number of spectral bands (three for visible range and one for NIR range) with a spatial resolution less than 10 meters. Along this way, the evolution has been incredible. Missions like SPOT5, Quickbird and Ikonos are still providing multi-spectral acquisitions at few meters of spatial resolution and panchromatic data at less than one meter. New applications and products have been developed and made available for the users such as satellite cartography and land cover maps at very high resolution.

Others optical sensors have been realized to satisfy the incoming needs concerning the monitoring of phenomena at very large scale. Events related to the photosynthetic conditions of the vegetation, wide deforestation and fires, desertification, sea pollution are playing an important role for the general health of the Earth and the assessment of these events is too much important to understand the impact which they could have on the fragile biophysical mechanisms. Regular (in most cases daily) observations of huge areas are needed and for this reason sensors like MERIS, MODIS, AVHRR and AATSR have been designed and placed in orbit. In these cases, the main property is not strictly related to the spatial resolution but rather to the swath width and to the revisit time. The measurements are performed using several spectral bands (up to 36 for MODIS) located into the visible and the infra red range in order to collect a noteworthy dataset for every kind of global investigation (land use, ocean color, snow cover, sea ice observation,...).

For a few others the technological improvements, pursuing the so-called hyper-spectral imagery, regard the spectral resolution and the allocation of

many contiguous and narrow bands (more than hundred) available for the measurement. The hyper-spectral measurements have demonstrated very high performances in several cases, for example sub pixel classification material identification and urban mapping. Indeed some of the last airborne payloads already include sensors with measurements carried out at thousands of wavelengths and at the finest spatial resolution. However, the development of this technology for the space satellites remains difficult and very expensive in terms of payload design, maintaining and calibration. In any case these difficulties have not deterred the space agencies to found interesting missions carrying on board hyper-spectral payloads. This is the case of Hyperion developed by NASA and CHRIS Proba-1 developed by an European consortium founded by ESA.

Proba-1 is the proof that the difficult hyper-spectral high resolution technology could be explored and proposed for the space satellites with a reasonable budget and satisfactory results. The compact spectrometer CHRIS can not properly be considered a pure hyper-spectral instruments like Hyperion, but its narrow and quasi-contiguous bands located in the visible and infrared ranges make this sensor closer to the hyper-spectral family than to the multi-spectral one. Moreover, the new innovations introduced in spacecraft design and tracking allow new manoeuvres during the target overpass, like the capability of tilt the satellite along the zenith and azimuth direction, providing hyper-spectral observations under different zenith angles. Other satellite missions have been providing information on the viewing direction and the directional anisotropy behavior of different surfaces. The MISR instrument on board NASA Terra platform acquires radiance data from any earth target in four solar spectral bands, from nine different directions, in at the most seven minutes, at a spatial resolution of 275 m in all bands of the

nadir camera and in the red band of the off-nadir cameras, and 1.1 km in the remainder [1], [2]. ADEOS-POLDER data are also an interesting example of multi-angle exploitation in remote sensing but, for their coarse spatial resolution, they are more suitable for monitoring atmospheric processes [3]. Higher spatial resolution multi-angular data have been provided by airborne campaigns such as DAISEX [4], or AMTIS [5] which however are characterized by localized and temporally limited acquisitions.

Therefore the PROBA mission and the CHRIS property of joining both hyperspectral and directional sampling with high spatial resolution represent a new promising scenario for the generation of land cover products from remotely sensed data. After 7 years of orbital life (initially intended as one year mission) the results produces by this mission have been important, not only for the development of new applications, but also for the testing of methodologies and algorithms for the future missions. In fact the scientific community has demonstrated an unexpected interest concerning this small satellite, requesting images and data in more cases over the real capability of this mission (in terms of daily acquisitions, ground segment, and observations planning). The incoming of new Proba missions with a new generation of CHRIS instrument, including more bands in the SWIR range, is strongly hoped and waited.

1.2 Aim of the thesis

This thesis proposes a complete investigation concerning the exploitation of the CHRIS images, starting from the pre application processing until the developing of the classification phases. Despite some processing steps are considered obvious for the optical products, some innovations have been im-

plemented and tested. For example the destriping process implements a methodology based on the filtering in the FFT domain and it seems to provide better results with respect to the others technique already applied to the CHRIS images.

The capability of the CHRIS land mode 3 spectral configuration for the production of land cover maps has been investigated and proposed in several exercises, using as well combinations of multi-angular and multi-temporal acquisitions as additional information for the classification. These exercises have been anticipated by a preliminary analysis that has outlined how different surfaces are characterized by a different spectral anisotropy. Moreover, simple multi-angular RGB compositions have demonstrated that this multi-directional factor can be used to better discriminate particular kinds of surfaces and structures.

Finally, a comparison between a land cover map generated using ETM+ Landsat and CHRIS Proba closes the work. This last exercises aims at evaluating the performances of CHRIS with respect to the most used multispectral sensor for classification purposes like ETM+.

1.3 Organization of the dissertation

This research work can be mainly divided in two part: the first part reports the phases related to the analysis and the processing of the optical data, while the second part in fully dedicated to the exercises of classification. Finally the conclusion are reported.

CHAPTER 1 (This one). It proposes a general introduction to the thesis.

CHAPTER 2. It reports a brief description of the Porba-1 mission and the small hyperspectral CHRIS. The target area is indicated and described in

terms of extension and land cover types. All the CHRIS datased available for this area is listed and critically discussed (season of acquisition, presence of clouds, translation of the frame,...) and also the others data used for the work are reported.

CHAPTER 3. Part dedicated to the pre application processing. In fact these images can not be directly used without some important and necessary processing steps. The first phases is dedicated to the radiometric correction with the black pixel removal and stripes equalization. Two methodology have been mainly tested and improved. After that, the atmospheric correction has permitted to calculate the surface reflectance starting from the radiance at the top of atmosphere. This has made possible comparisons and exercises based on the joined use of multi-angular and multi-temporal acquisitions. Finally the geo-rectification has permitted to integrate the analysis with other image and information layers available for the test area.

CHAPTER 4. Fully dedicated to the classification. A preliminary visual and spectral analysis introduces the concept of spectral anisotropy for many surfaces. After that, the classification exercises, performed with different configurations of inputs, have highlighted the potential of these new spectral and geometric acquisitions to improve the accuracy of land cover maps.

CHAPTER 5. This part reports the conclusions and the final consideration regarding this research work. Each step of processing is reviewed and critically discussed and the points for the future development are individuated.

Chapter 2

CHRIS Proba acquisitions over Frascati and Tor Vergata

2.1 The Proba-1 mission and the small hyperspectral CHRIS

The project for On-Board Autonomy (Proba-1) satellite was launched in the 2001 with the principal aims of developing new technologies and solutions in platform design, space navigation and orbit tracking and maintaining. This mission was founded by an European consortium and it was planned with the initial orbital life of 1 year. But following the encouraging results provided since the beginning, associated with a good status of systems and sensors included into the payload, this mission has been maintained operational and new acquisitions and manoeuvres are still planned.

The payload includes several earth observation and space environment scientific instruments, but many elements and systems inside the spacecraft have been included as technology experiments. The two most important earth

observation sensors are the panchromatic camera HRC and the small hyperspectral CHRIS. CHRIS provides acquisitions up to 62 narrow and quasi

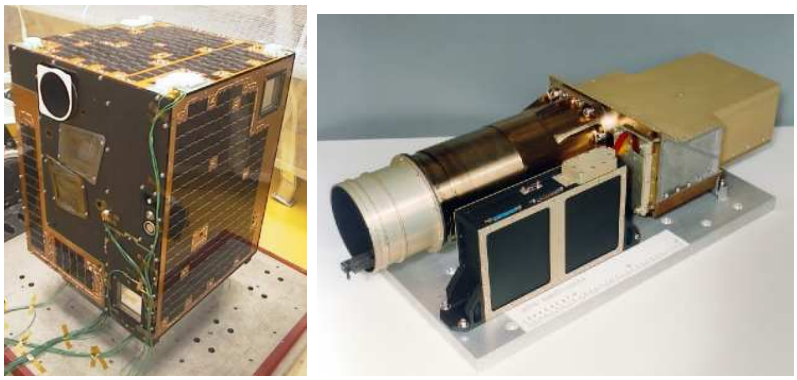

(a) (b)

Figure 2.1: (a) PROBA satellite, (b) CHRIS sensor

contiguous spectral bands with the spatial resolution of 34-40 meters and a radiometric resolution of 5-10 nm. It is also possible the planning of observations with an increased resolution of 17-20 meters using only a subset of 18 spectral bands [6]. In fact CHRIS is characterized by different operational modes, that are associated to each spectral configurations how is outlined below.

Mode 1: full swath, reduced resolution. CHRIS acquires image data across 13 km of nominal swath with 62 narrow spectral bands at 34 m of nominal spatial resolution.

Mode 2-4: full swath, full resolution. CHRIS acquires images characterized by 17 m of nominal spatial resolution, 18 spectral bands and 13 km of nominal swath width. In this case, different combinations of the 18 spectral bands identify different missions: *Mode 2* for investigations regarding water bodies, *Mode 3* for land uses studies and aerosols properties retrieval and finally *Mode 4* for chlorophyll content retrieval.

Mode 5: half swath, full resolution. This operational mode provided acquisitions of half swath image at full resolution with a combination of 37 spectral bands.

The principal innovation of this satellite consists in tilting the spacecraft on two axis, along- and across-track, during the target overpass, allowing quasi-simultaneous acquisitions under five different zenith angles (FZA +55, +36, 0, -36, -55). In fact, each imaged target will have an associated "fly-by" position and this is the position on the ground track when the platform zenith angle, as seen from the target, is a minimum zenith angle(MZA). The platform acquires the images at times when the zenith angle of the platform with respect to the fly-by position is equal to a set of Fly-by Zenith Angles [7]. For this reason each acquisition produces a dataset composed by 5 images related to the tilted observations. This multiple-view-angle (MVA) imaging capability, in addition to the high spectral and spatial sensor resolution, permits the collection of a large amounts of data in order to perform new studies regarding the lands, water surfaces and the atmosphere. The Fig. 2.2 represents the angular positions during the observation with respect to the target [8]

2.2 The test area of Frascati and Tor Vergata

Proba performs acquisitions (CHRIS and HRC) over several specified test areas around the world. The area where the Campus of Tor Vergata University is located is actually one of the test site for this mission and it includes also the area of vineyards located on the rural site of Frascati. This test site is narrowed on the south by the area of Ciampino, on the north by the zone of Casilina street, on the est by the area of Pantano Romano and finally it

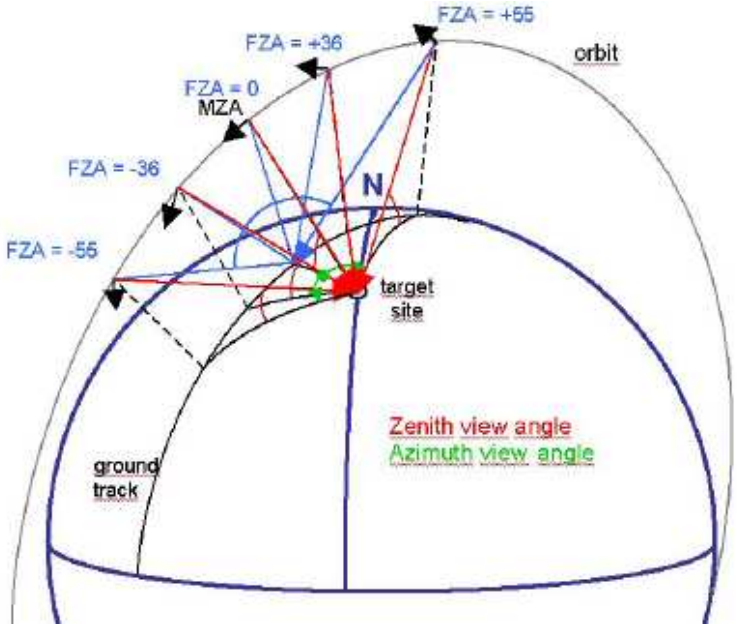

Figure 2.2: Multi-angle acquisition during the target overpass

arrives until the Grande Raccordo Anulare of Rome along the west direction. This area is interesting for its very heterogeneous environment, in fact it is possible to find different kinds of man made surfaces and structures (modern and historical), which are mixed with rural areas composed by permanent crops (vineyards and olive trees) and different cultivated fields under yearly rotation of plugging and growing phases (principally corn, vegetables and others cultivations). Asphalted surfaces are present in streets of various size such as motorway, secondary and state streets, which cross fully urbanized quarters with residential houses, flats and big industrial/commercial units with large parking areas and squares. The Fig. 2.3 shows the maps of the main area of interest.

(a)

(b)

Figure 2.3: (a) Maps of the area of interest (from Google Maps), (b) VHR Quickbird image over the same area

2.3 Acquisitions in mode 3 spectral configuration

Several CHRIS Proba acquisitions have been planned since December 2004, using the mode 3 spectral configuration at 18 meters of spatial resolution. This spectral configuration is particular useful to perform investigations regarding land use, land changes and for the monitoring of the vegetation status. The table 2.1 indicates the spectral configuration of CHRIS Mode 3 [7] Considering its spatial resolution, CHRIS could be included in the same family of Lansat ETM+ and SPOT4 (20-30 meters), but the new band configuration in terms of spectral sampling and bands narrowing, makes this sensor closer to an hyperspectral instrument than a pure multi-spectral ones. The CHRIS range of acquisition arrives until 1035 nm (VISIBLE + NIR) while Landsat ETM+ and SPOT HRVIR have bands also into the SWIR range. But the principal difference consists on the sampling of the acquisition spectral range in very narrow and quasi-contiguous bands, with the principal aim of a better identification and discrimination of spectral signatures related to different surfaces. CHRIS has also two narrow bands located around the 442 and 490 nm, which are particularly useful for the aerosols properties retrieval, especially if they are analyzed considering all the multi-angular acquisitions. The introduction of very narrow bands into the red edge range (700-800 nm) is one of the principal innovation proposed by the CHRIS land mission, allowing a better identification of vegetated surfaces and permanent crops. Finally the narrowing of the spectral bands permits to minimize the effects related to the aerosols and water vapor scattering and absorption.

The FIg.2.4 depicts the spectral allocation of CHRIS and Lansat ETM+.

Band	Min λ	Max λ	Mid λ	Width
L1	438	447	442	9
L2	486	495	490	9
L3	526	534	530	9
L4	546	556	551	10
L5	566	573	570	8
L6	627	636	631	9
L7	656	666	661	11
L8	666	677	672	11
L9	694	700	697	6
L10	700	706	703	6
L11	706	712	709	6
L12	738	745	742	7
L13	745	752	748	7
L14	773	788	781	15
L15	863	881	872	18
L16	891	900	895	10
L17	900	910	905	10
L18	1002	1035	1019	33

Table 2.1: Spectral configuration of CHRIS Mode 3 (values expressed in nm)

The CHRIS bands cover the spectral range between 443 and 1019 nm while ETM+ has only four bands inside this range (Blue, Green, Red and NIR) with other two more bands at 1650 nm and 2221 nm.

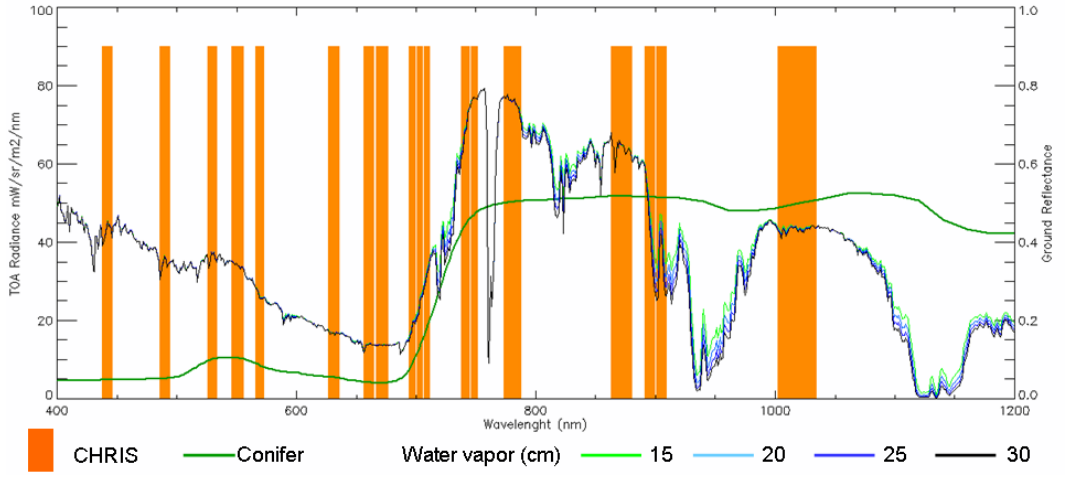

(a)

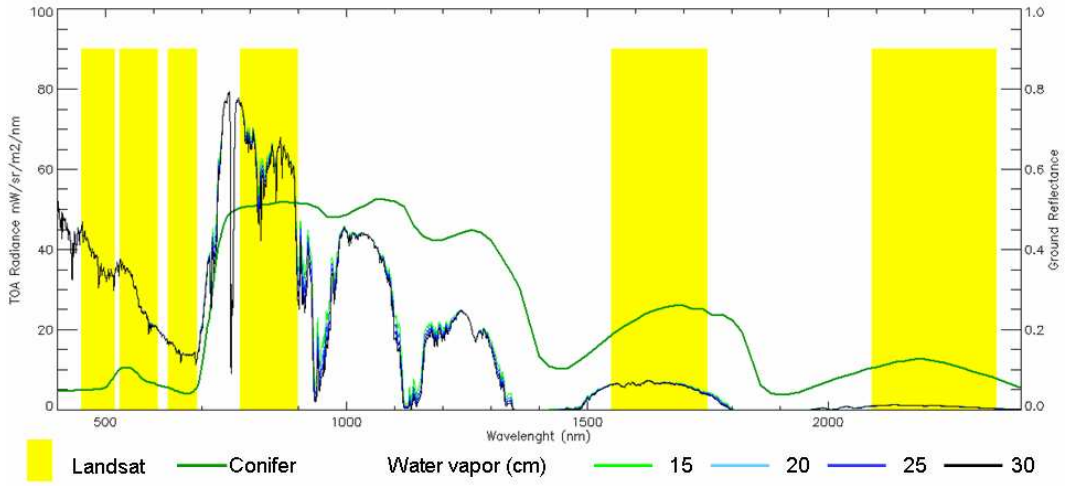

(b)

Figure 2.4: (a) CHRIS mode 3 bands allocation, (b) Landsat ETM+ bands allocation

2.4 Data used for the work

The dataset is composed by a collection of optical products, which are characterized by different spatial resolution and different spectral band config-

uration. The CHRIS acquisitions cover a temporal range since December 2004 until the 2007 and new observations are still planned. How is possible to see in Tab. 2.2, several acquisitions have been done in three years, but unfortunately most of them are related to the winter season and during the months of December, January and February (or closer). Moreover, others difficulties due to the geometry of acquisition, frame shifts and cloud cover have limited the analysis to only some acquisition dates. The image ancillary data are not available for all the images and for this reason the year 2004 has been partially considered for this work. Some Landsat ETM+ images

Year 2004	Year 2005	Year 2006	Year 2007
15 December	1 March	7 January	30 January
23 december	8 March	28 February	16 February
	1 June	19 August	24 May
	30 December	9 October	4 November
		11 November	

Table 2.2: CHRIS Proba acquisition available for the area of Frascati and Tor Vergata.

acquired over the center of Italy have been used to perform analysis finalized to asses the spectral differences with respect the CHRIS products. They are related to the dates 9 July and 3 August 2001 (made available by the GLCF project) and 19 August 2004 courteously provided by ESA.

Very high resolution images have been also included on this dataset, in particular the Quickbird pan-sharpened images at 1 meter of spatial resolution and PROBA HRC panchromatic images at 5m of spatial resolution. In particulat the Quickbird products, acquired during the 2002 and 2005 respectively, have been used to rectify the CHRIS images and to collect areas and surfaces for

the training of the classification process and to validate the results.
Others auxiliary products have been included into the dataset such as GIS data and on ground measurements. Vector layers like CLC 2000 and vineyards polygons have been registered and overlapped to the remotely sensed images in order to better characterize the scenario and to discriminated cultivated areas from natural and not used zones. Aerosols on ground measurements, which have been carried out at CNR of Tor Vergata, have been also considered for the atmospheric corrections.

Figure 2.5: VHR Quickbird images with the vineyards polygons

Chapter 3

Pre-application processing

3.1 Introduction

Before showing the results obtained by the use of the new CHRIS images for the specific application, some correction steps have to be reported because necessary to solve several radiometric and geometric uncertainties still presents in the products. In particular black pixel and stripes correction are performed to compensate corrupted pixels and noisy columns while the atmospheric correction is carried out to delete the radiance due to the interaction of the measured signal with the atmosphere. Finally the ortho-rectification, performed using the polynomial method with GCPs has permitted to register spatially the images and the others layers used for this work.

3.2 Black pixel removal

Pixels without information (pixel with 0 value), placed along the row with a periodic structure, have been found in the CHRIS Proba images. This noise is present in different bands and in different row positions. It is possible to

associate an estimated value to the corrupted pixel applying an average filter around the black pixel. A dedicated routine, which automatically finds the bad pixels in each band of the hyperspectral data and computes the mean value around them has been developed to eliminate this kind of noise. The mean is within into a 3x3 moving window centered in the bad pixels.
The routine is adaptative, because the pixels with zero value are often present along the image edges (top edge or/and bottom edge) and along the rows near the edge. For this reason the routine makes firstly a check over the image edges and, for the selected bad pixels computes, the mean using special windows. After that the routine works in normal mode with the 3x3 window. The Fig. 3.1 shows and example of lines corrupted by the presence of black pixels.

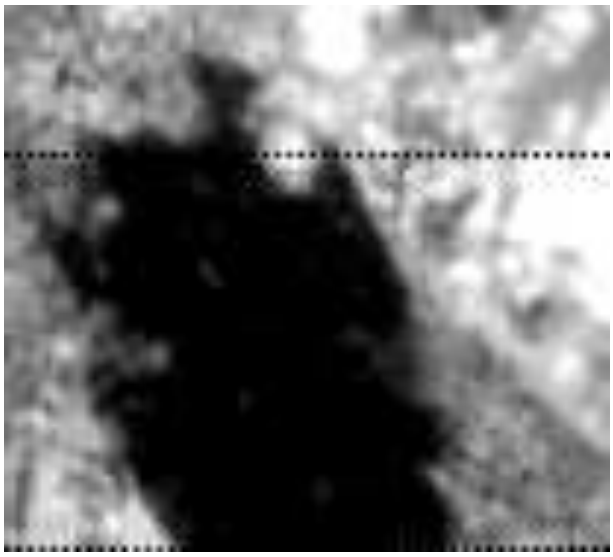

Figure 3.1: Example of rows with black pixels, one along the bottom edge and the other inside the scenario

3.3 The stripes noise in the optical images

The problem of stripes consists in strong variations in the average value in the column for every band of CHRIS Proba images. This noise affects all the optical instruments which perform the scanning phase using detectors organized in line or registers. For example the push-broom sensors have the electro/optical detectors organized following the structure of a 2-dimensional array, where each row scans spatially the scenario at one wavelength producing the digital row image (or called sub-image) related to a particular band. The detectors, that compose the spectral arrays, are well calibrated to provide the same outputs if illuminated with the same radiance, but unfortunately a residual non-uniformity of the electro/optical response is still present. In particular the gain of each detector results different from the others and for this reason stripes appear along the scanning direction with a different distribution inside the image and a different band positions [9]. Moreover, thermal fluctuation during the orbit causes additive small variations in the alignment of the detectors, producing a not predictable noise which do not stay constant during the time [13]. Only the systematic knowledge of the gain function permits an accurate compensation of these fluctuations. The electro/optic response could be calculated analyzing the outputs provided by the detectors if illuminated with the same radiance (on-board lamps and devices or known target in the scenario). This methodology is difficult to apply systematically during the satellite life and for this reason the image processing remains one of the best solution for this problem. It is possible to divide the methodologies in three classes: algorithms based on spatial filtering, histogram modification [9] and and algorithms based on advanced filtering such as the filtering of the power spectrum [10] and by the use of wavelet transform [11]. Moreover since November 2006, a freeware tool for

the image radiometric reprocessing has been made available by SIRA Space [12] under the CHRIS Proba project. For this work the methodologies based on the histogram modification and power spectrum filtering have been implemented and improved for CHRIS. The histogram modification has not used any more in favor of the power spectrum filtering, because the last method seems to provide better results for our scenario. In any case, the use of a coupled processing, composed by the power spectrum filtering as the first step with the histogram modification as second step, is often suggested in order to improve the correction.

3.4 Destriping based on the histogram modification

The purpose of this equalization is to modify the histogram of the striped images to perform the noise reduction. It is based on the assumption that all detectors acquire sub-images with the same statistic distribution and this condition is verified when the scenario presents large parts characterized an homogeneous environment. Under this assumption, the local histogram of each sub-image, which has been acquired by every detector, can be statistically matched with the global histogram of the entire image. This produces an effect of mitigation for the stripes.

The correction is performed applying the linear relation which links the radiance captured by detectors with their outputs in function of gain and bias. In general, the detector of the register b, related to the column n in the band k, which acquires a signal o radiance L, it produces an output $X_{n,k}$ that could

be represented by the linear equation [14]:

$$X_{n,k} = G_{n,k}.\gamma_{b,k}.g_{b,k}.L + C_{n,k} \tag{3.1}$$

where $G_{n,k}$ is the gain associated to the detector n for the band k, $\gamma_{b,k}$ is the inter-register gain, $g_{b,k}$ is the inter-detector gain and $C_{n,k}$ is the bias associated to the detector. The correction is done by the estimation of gains and bias for each detector and the correction factor could be calculated and applied to all noisy columns. In general gains and bias are obtained acquiring images over dark targets (images during the night) and over very homogenous scenarios (deserts, ice, sea) but this operations can not be done systematically by the satellite. Moreover, the correction factors calculated for one orbit cannot satisfactory compensate the noise in images acquired during the following orbits. For this reason gains and bias have to be calculated directly using the statistics of the images. A destriping tool based on this kind of approach has been implemented and tested for our dataset.

We pone the inter-register and inter-detector gain equal to one and considering L the pixel of radiance which compose the column n of the spectral band k, it is possible to carry out a the recalibration equation to apply to each column:

$$Y_{n,k} = G_{n,k}.L + C_{n,k} \tag{3.2}$$

where $Y_{n,k}$ represents the corrected pixel of the column under equalization. The gain $G_{n,k}$ and the bias $C_{n,k}$ are tuned comparing the statistics of the column under correction with the statistics of the whole image. In fact it is possible to have:

$$G_{n,k} = \frac{\overline{s_k}}{s_{n,k}} \tag{3.3}$$

and

$$C_{n,k} = \overline{m_k} - G_{n,k}.m_{n,k} \tag{3.4}$$

where $\overline{m_k}$ and $\overline{s_k}$ are the mean and the standard deviation of the whole image, $m_{n,k}$ and $m_{n,k}$ are the mean and the standard deviation of the column n under equalization.
This methodology has provided good results in many cases and also the algorithm is simple to apply, but some disadvantages have been observed:

- The algorithms is strongly image dependant and at same time the sub-image statistics can not be matched with the statistics related to the entire image
- Wide areas characterized by different surfaces (snow, clouds, very dense urban quarters) could be sources of errors during the correction phase
- In some cases the correction could impact on the radiometric information.

3.5 Destriping based on the filtering in the frequency spatial domain

This method considers the stripe noise as a multiplicative factor for the image column which produces strong variations among pixels of adjacent columns. These variations can be seen in frequency domain as the presence of high frequency components in the power spectrum computed over the column averages (FFT over the column averages). Then it is possible to mitigate these components through a low-pass filtering.

This algorithm has been proposed by M.J.Settle [13] and includes some important steeps:

1. For each band, calculate an average radiance for each column of data
2. Calculate the logarithm for these averages
3. Apply a low pass filter to cut the high frequency components
4. Subtract the result of step from the logarithm of averages to obtain the correction factors.
5. Calculate the anti-logarithm.
6. Apply the correction factors to each column of the image.

The destriping tool developed for CHRIS implements these steps improving some phases and introducing new functionalities to avoid residual radiometric artifacts. The step 3 in now performed after the transformation of the averages from the spatial domain to the frequency domain by the use of the discrete 1-D FFT. This has permitted to isolate better the noise, observed as the presence of high frequency components, giving more effectiveness to the filtering phase. The filter itself is a now a Butterworth low-pass filter [15] with the possibility of configuring its parameters in input (magnitude and cut-off frequency) to obtain a good correction. The last evolution of this methodology includes a new functionality for the masking of bright and dark pixels. In fact, it has been observed that for columns partially characterized by the presence of very heterogeneous areas, such as shadows and clouds, the correction remains incomplete. For example, image portions interested by groups of clouds and shadows, a not corrected noise remains in cloud free areas along the column direction and it appears like blurred dark stripes.

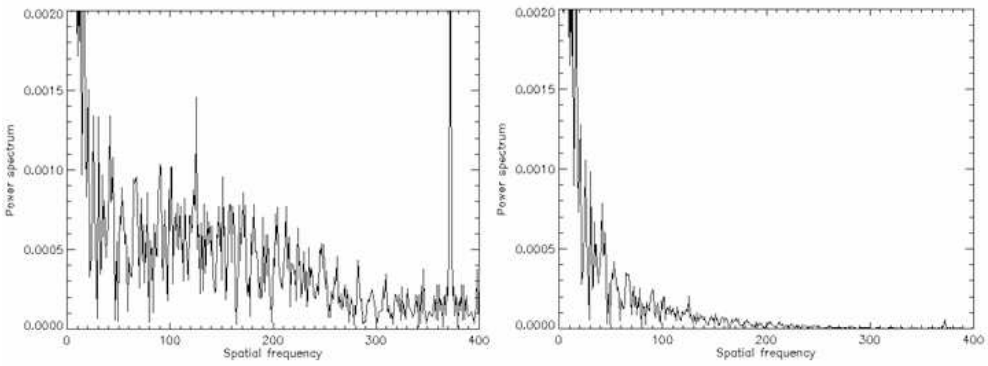

Figure 3.2: Example of power spectrum affected by striped (left) and power spectrum after the correction (right)

The new functionality has the purpose of masking these noisy zones, trying to not include pixels of these heterogeneous areas for the computation of the column means. The improved version of this methodology introduces new phases between the step 1 and 2:

- For each band, the standard deviation has been calculated for all the columns
- The standard deviation is used to define new ranges of values which does not include brightest pixels.
- New columns means are calculated inside the new ranges of value

In others words, the definition of a new range of values permits to obtain column means less affected by the presence of pixels belonging in sub-images statistically different from the others. The extent of this range can be defined in input (in function of the standard deviation) and it can be properly modified to reach a good correction. Tests performed over several images have demonstrated a good correction with ranges that consider pixel values inside the standard deviation.

Fig. 3.4 and Fig. 3.3 show two examples of CHRIS striped and detriped

band 1 for images acquired over the Libyan desert and over Tor Vergata campus. The visual assessment confirms a satisfactory denoising keeping a good presence of details, without blurring effects also in areas with high spatial frequency. The statistical analysis, which has been carried out for the Frascati/Tor Vergata test site and reported in Tab. 3.1, demonstrates a very low impact on the radiometric information having not relevant changes in the image statistics for all bands. The Fig. 3.5 reports the same scenario where the noise are not perfectly corrected for columns partially covered by clouds and shadow (on the right side). The bright pixels masking has permitted to have better results for these areas and no residual stripes are observed. On the other hand, the Fig. 3.6 shows a missing stripe equalization for columns composed by pixels of different surfaces along the on track direction. This scenario is a very difficult example and it is typical for acquisitions over islands, ports or costal areas with a large parts covered by the sea. For these cases the correction remains difficult and for some areas not satisfactory. The tuning of parameters related to the correction (filter parameters, ranges for the extraction of the mean) can attenuate the noise, but blurred stripes could remains uncorrected.

(a)

(b)

Figure 3.3: Image acquired over the Lybian desert (band 1): (a) original image affected and disequalized by the presence of stripes, (b) the same image after the destriping

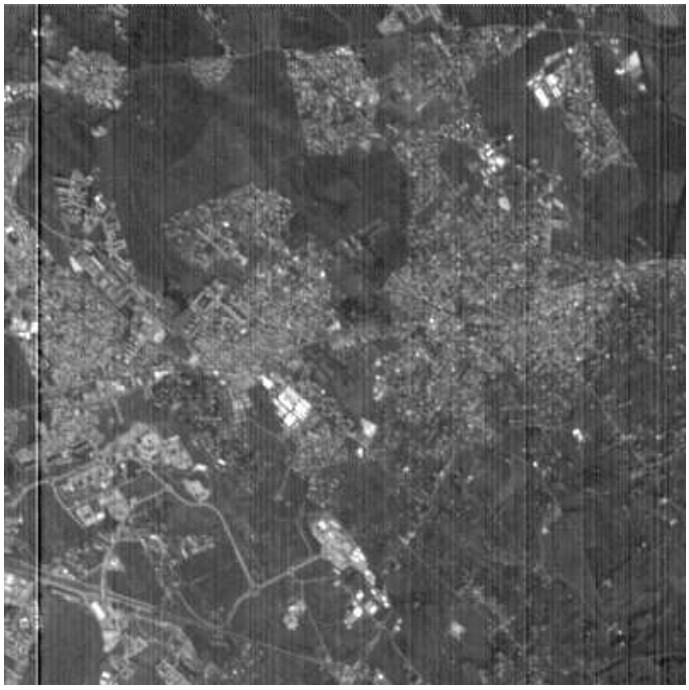

(a)

(b)

Figure 3.4: (a) Band 1 of CHRIS image acquired on 30 January 2007 affected by stripes, (b) the same image after detriping

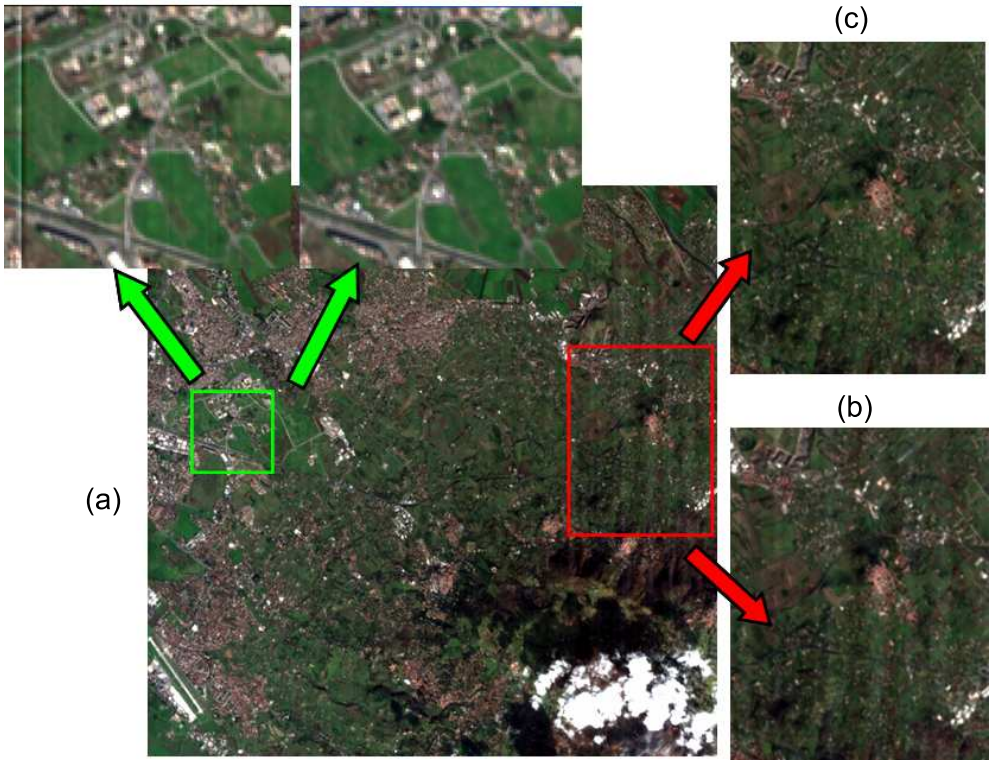

Figure 3.5: (a) CHRIS image of 30 January 2007, (b) area affected by residual stripes close to a cumulus of clouds, (c) the same area mitigated by the use of the bright pixels masking

(a) (b)

Figure 3.6: Tampa Bay (USA), missing correction close to the coast line

Band	Mean original	Stdev original	Mean destriped	Stdev destriped
Band1	51.264	5.519	51.247	5.336
Band2	41.747	6.874	41.740	6.727
Band3	36.042	6.892	36.031	6.765
Band4	35.928	7.411	35.920	7.282
Band5	31.025	7.025	31.020	6.912
Band6	25.796	7.368	25.794	7.278
Band7	24.825	7.851	24.824	7.758
Band8	24.707	8.182	24.706	8.090
Band9	26.878	7.027	26.879	6.940
Band10	31.249	7.437	31.247	7.336
Band11	31.861	7.399	31.855	7.310
Band12	43.826	12.017	43.797	11.928
Band13	42.720	12.058	42.688	11.968
Band14	44.117	12.641	44.080	12.553
Band15	40.131	11.642	40.096	11564
Band16	33.958	9.738	33.933	9.671
Band17	30.219	8.601	30.196	8.535
Band18	39.401	10.497	39.363	10.423

Table 3.1: Global statistical analysis performed for the image of 30 January 2007

3.6 The atmospheric correction

Another important step of the pre-processing phase regards the atmospheric correction. This step plays an important role in our applications, because the merging of images acquired under different angles of view and in different dates requires systematic compensation of the atmospheric effects which are strictly dependent on the geometry of the acquisition and on the seasonal condition. The first issue consists in estimating the contribution of the atmospheric effects in terms of total irradiance, direct and diffuse transmittance and radiance due to the atmospheric scattering. These parameters are related to the acquisition day (solar irradiance, position of the Earth with respect to the sun), to the atmospheric conditions (aerosols concentration, water vapor content, chemical profile of the atmosphere, profile of temperature and pressure) and to the geometry of the acquisition (zenith and azimuth angle of view, time of acquisition, position of the satellite with respect to the sun). The estimations have been produced starting from simulations carried out with the suite of libraries Libradtran, for the simulation of the radiative transfer balance [16]. In particular the tool uvspec has been used to produce the simulated raditiave quantities for each wavelength, receiving like input series of parameters regarding the acquisition time, the satellite position and the atmospheric characterization. The table 3.2 summarizes some significant inputs required for the simulation [17]. In order to perform the simulations, standard seasonal profiles for the atmosphere have been considered while the aerosols characterization, in terms of Aerosol Optical Thickness (AOT), Single Scattering Albedo (SSA) and Angstrom coefficients, has been obtained by the use of measurements performed by the sun-photometer at CNR Tor Vergata and available under the NASA Aeronet Project [18]. Also for the water vapor content, the measurements delivered under the same project

Atmosphere	Seasonal atmospheric profiles (temperature, pressure, gas concentrations), gas absorption parameters (HITRAN, LOWTRAN, SBDAR)
Aerosols	Aerosols type below and above 2 km, AOT at 550 nm, SSA, single or multiple scattering
Water vapor	Water vapor content
Spectral information	Wavelength range, convolution filter, spline interpolation
Acquisition geometry	Altitude, OZA, OAA
Solar information	Day, time, latitude and longitude of the target
Equation solver	radiative transfer equation solver rutines (disort, disort2, polradtran,...)
Output	Radiances, transmittance, irradiance

Table 3.2: Significant inputs for the radiative simulations

have been included.

The correction and the $\rho(\lambda, \theta)$ reflectance calculation has been performed implementing the following relation:

$$\rho(\lambda, \theta) = \frac{\pi(L_{TOA}(\lambda, \theta) - L_{path}(\lambda, \theta))}{E_0(\lambda, \zeta)\, T(\lambda, \theta)} \tag{3.5}$$

Where $L_{TOA}(\lambda, \theta)$ is the radiance at the top of atmosphere captured by the sensor, $L_{path}(\lambda, \theta)$ is the radiance contribution due to the scattering along the target/sensor path, $E_0(\lambda, \zeta)$ is the total irradiance calculated at the top of

Figure 3.7: Effects of adjacency correction. Particular before the correction (on the left) and after the correction (on the right)

the canopy and finally $T(\lambda, \theta)$ is the total transmittance along the path target/sensor. After that, the adjacency correction is performed by a weighted average applied to all pixel for the pixel [19]

$$\rho^2(x,y) = \rho^1(x,y) + q\{\rho^1(x,y) - \overline{\rho}(x,y)\} \tag{3.6}$$

where

$$\overline{\rho}(x,y) = \frac{1}{N^2} \sum_{i,j}^{N} \rho^1_{i,j}(x,y) \tag{3.7}$$

Where $\rho^2(x,y)$ is the corrected pixel reflectance, $\rho^1(x,y)$ is the uncorrected pixel reflectance, q is the ratio between the diffuse and direct transmittance and $\overline{\rho}$ is the mean reflectance calculated in a moving window of NxN pixels. Good results have been obtained using $N = 11$.

3.7 The geo-rectification

Once calibrated, the images had to be co-registered. The coregistration of all images, and in particular of those taken at different incidence angles has been

one of the most delicate step and has been preliminary to the multi-angular analysis and to the subsequent classification procedure. We considered as master the image taken with the larger acquisition angle and, before starting the coregistration, all other images have been resized to have the same spatial resolution. This led to have a pixel size of 23 meters for all considered images, which degrades softly the spatial resolution of nadir images but allowed us a good overlapping among different angle acquisitions.

Finally the images have been rectified using a semi-automatic methodology based on the manual selection of Ground Control Points [20] and taking as master a very high resolution (VHR Pansharpened Quickbird image (0.63 m resolution) acquired over the same area in February 2002. On its turn the master image has been previously rectified with several GPS Ground Control Points. A final geometric precision of less than one pixel (calculated over the GCPs) has been achieved which can be recognized as satisfactory for this context.

Chapter 4

The production of land cover and land use maps

4.1 Introduction

After many correction steps, this chapter is dedicated to the classification applied to the CHRIS images. This investigation aims at discovering and analyzing the potentialities provided by these spectral and quasi-simultaneous multi-angular acquisitions for the production of land cover and land use maps for the area of Frascati and Tor Vergata. Preliminary visual and spectral analysis have encouraged the investigation towards the integration of multi-angular and multi-temporal information with the single nadir image, that is the one commonly used for the classification. Some classification exercises have been proposed using these additional angular and temporal information as support for the decision phase. The difficulties encountered during the images integration (very tough co-registration, finer atmospheric correction, pixel resampling, evaluation of residual distortions and shifts) have been compensated by important results which have permitted to asses the

impact of joined spectral, angular and temporal information for this kind of application. The examples proposed on this work seem to justify a strong technological effort towards hyperspectral, multi-directional and high revisit time satellite, but the real improvement for the end user applications shall be well analyzed. For this reason the classifications performances of Landsat ETM+ an CHRIS Proba have been verified and correlated over the same test site. The results have been proposed at the end of this chapter as a preliminary comparison between the commonly used mission for classification like Landast and the new improved payload and instrument like CHRIS.

4.2 Preliminary multi-angular analysis

The results stemming from a multi-spectral and multi-angular reflectance analysis are reported and critically discussed for several surfaces, which are typically included in many classes of land cover [21].

The first investigation aims at discovering differences over natural and man-made surfaces in terms of multi-angular acquisitions considering the same spectral band. The first example reported in Fig. 4.1 focuses the area of Tor Vergata University. In this case two different multi-angular compositions have been generated considering the band 10 (703 nm). We can appreciate how some features can be better retrieved in the angular compositions (b) and (c) with respect to the true color image (a). For example the multi-angular compositions allow a clearer perception of differences in vegetation density. Areas of bare soils (dark areas in b and c) are more visible as well, especially considering the composition (c). The urban structures can be well discriminated using the composition (b) and (c) and it is possible to perform a preliminary distinction among different kinds of buildings. In fact,

the residential buildings appear in a different color (green in b and red in c) with respect to the brighter commercial and industrial buildings. Indeed industrial and commercial blocks are in general characterized by less complex geometry and smaller height with respect to residential buildings. This could yield different values of the reflectance in the multi-angle acquisitions.

A second example is proposed Fig. 4.2 where some fields of maize have been observed. In this case the multi-angular composition (b) reports two different responses for the reflectance values inside the big triangular fields, while observing only the true color composition, the division in two adjacent fields is not so evident (a). This could be due to a different stage of cultivation or plants grow, which can be better appreciated considering the multi-directional reflectance rather than only using the spectral information. The very high resolution image confirms that the field is really composed by two different areas. After this visual analysis, several polygons, representing different typologies of land cover classes (vegetated areas, permanent crops, asphalted surfaces, buildings), have been selected from the images and the angular signatures of the reflectances plotted. The polygons have been extracted from the inner part of the area of interest to minimize the effects of the surroundings.

The signature of two types of crops (Fig. 4.3), of two types of vegetated areas (Fig. 4.4), of two urban zones with different structures (Fig. 4.5) and of two types of asphalt coverage (Fig. 4.6) are reported. All 5 different angle acquisitions are considered and analyzed. The Fig. 4.3 shows that the reflectance values calculated over row vineyards have more sensitivity to the angle of acquisition than those of corn field. In fact, this crop is characterized by a particular geometric distribution of plants (along rows separated with a distance of 2 meters) while for the corn the distribution

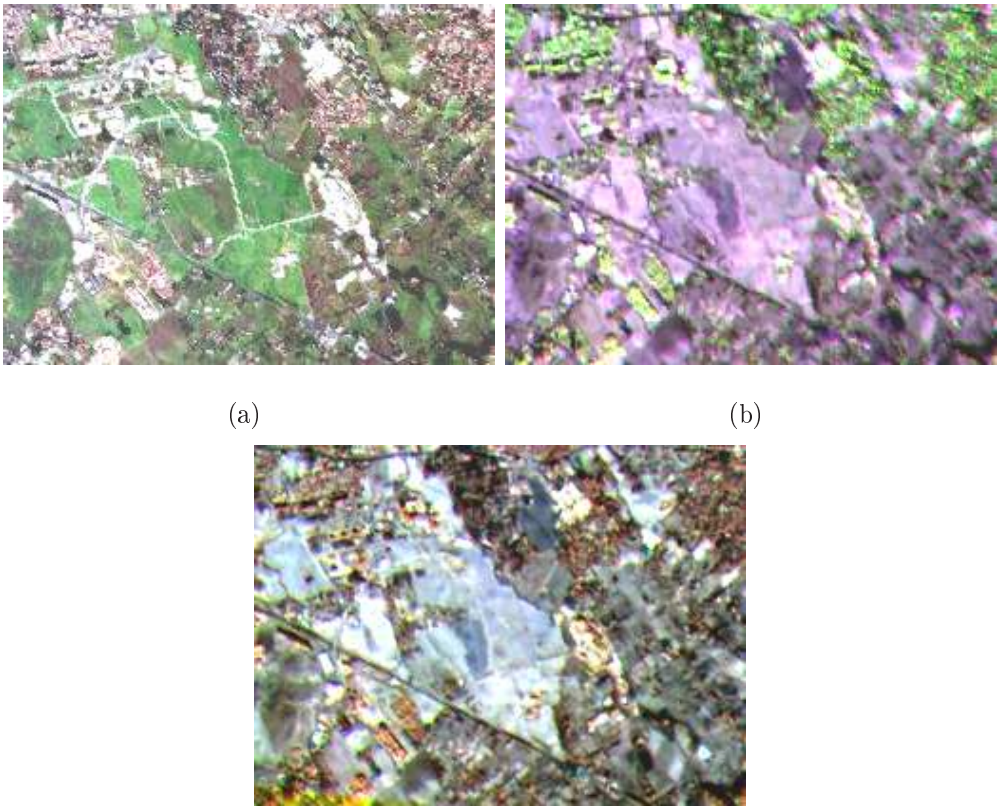

(a) (b)

(c)

Figure 4.1: Tor Vergata University campus: (a) true color composition using band 8, band 4, band 2, (b) RGB angular composition using band 10 and FZA-36, FZA0 and FZA36, (c) RGB angular composition using band 10 and FZA0, FZA36 and FZA55

of canopies is homogeneous and very dense, especially during the growing phase in summer. For vegetated areas, a similar trend with angle variation is observed and two examples related to dense forest and uncultivated areas are reported. Comparing with the vineyard, the others vegetated areas seem to have less sensitivity with respect to the direction of view. Comparing the multi-directional signatures of all vegetated areas, it results that the cultivation action introduces an important angular sensitivity, which varies among the crops types. In particular, for crops characterized by a precise geometric

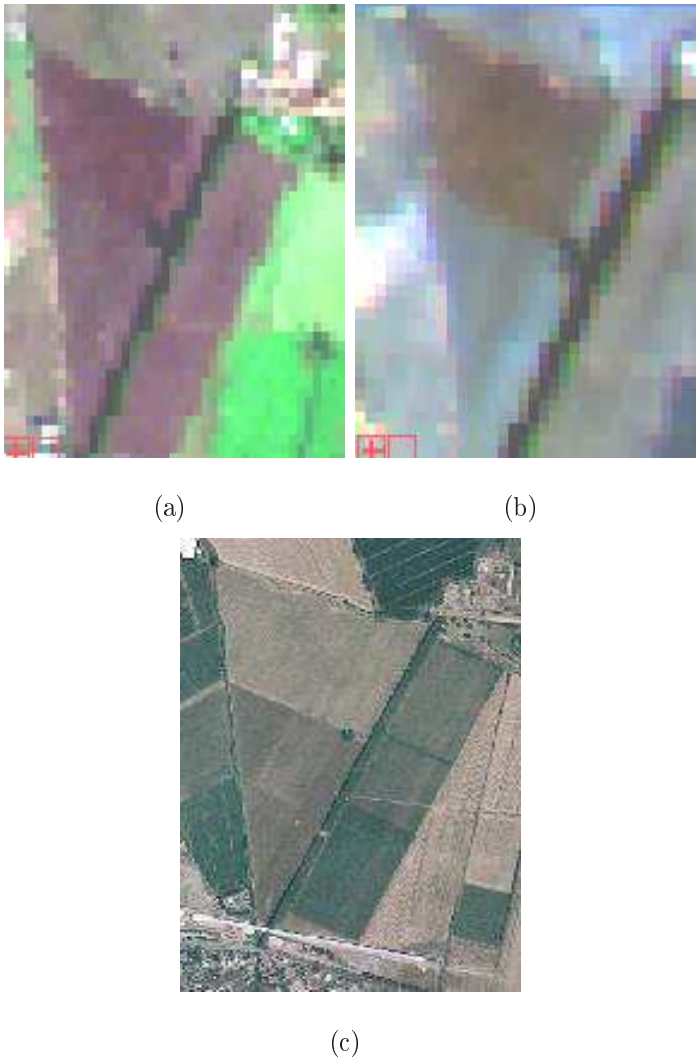

(a) (b)

(c)

Figure 4.2: Fields of maize: (a) True color composition using band 8, band 4, band 2, (b) RGB angular composition using band 10, (c) very high resolution image

structure, such as the vineyards or fruit trees, the angle of acquisition could significantly impact the measurements of the top of canopy reflectance. Considering urban areas in Fig. 4.5, both residential buildings and commercial/industrial units present a large sensitivity of the reflectance with respect to the angle of acquisition. In particular for commercial and industrial structures we can see that rather high values in the spectral signature have been

measured for the image related to the acquisition of FZA 36°.

Results concerning asphalted surfaces are shown in Fig. 4.6. In both cases, the spectral signatures extracted from all multi-angle images are rather close together. This confirms that the flatness characterizing such surfaces lowers the directional sensitivity of the reflectance. However, for longer values of wavelengths the bright asphalted surfaces (secondary roads, urban parking areas) exhibit very little sensitivity to the acquisition angle. Conversely, for dark asphalt covered surfaces (motorways, state highways), a significant dependence of the signature for the whole considered spectral range can be noted for FZA-55, while for the others angles the signatures are very similar. Considering the visual analysis as well as the statistic one, it is evident that the multi-directional view can provide more information regarding the nature of surfaces under observation and it can be added as additional information in support to the classification processing.

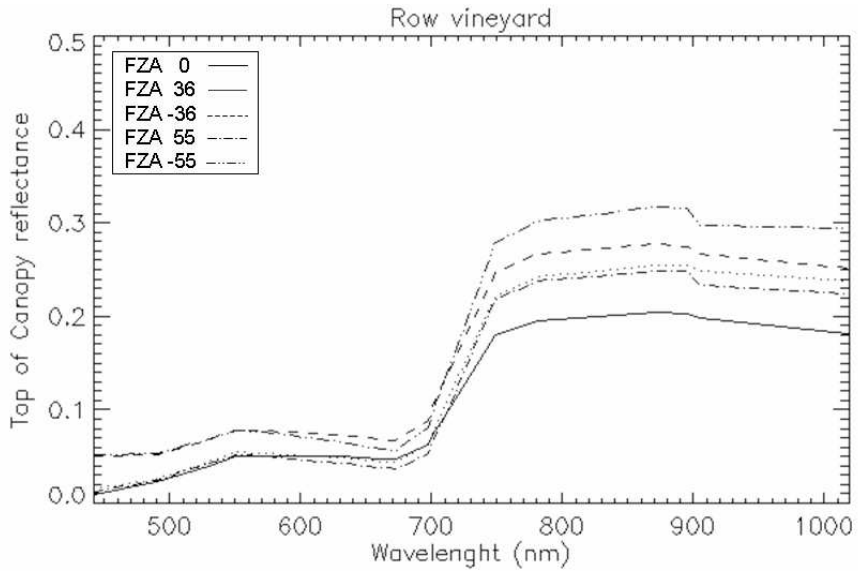

(a)

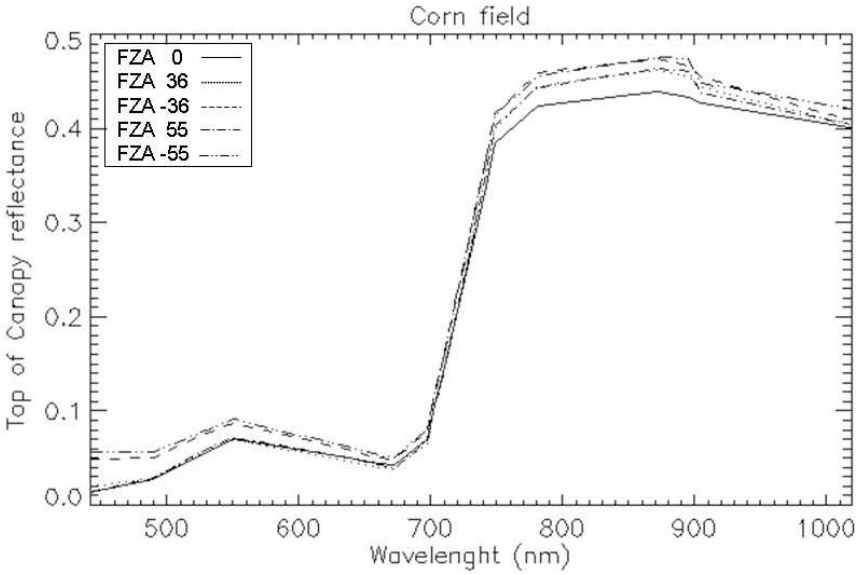

(b)

Figure 4.3: (a) multi-angular reflectance for a row vineyard, (b) multi-angular reflectance for a corn field

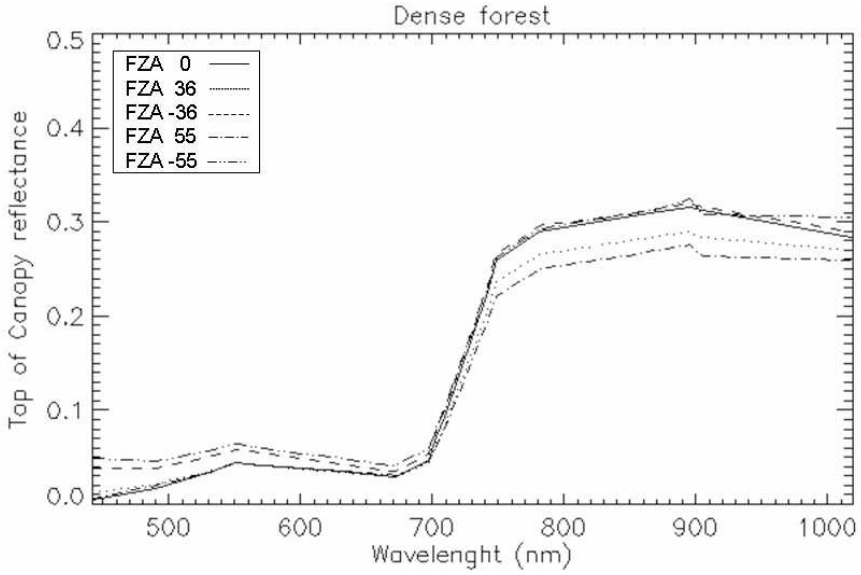

(a)

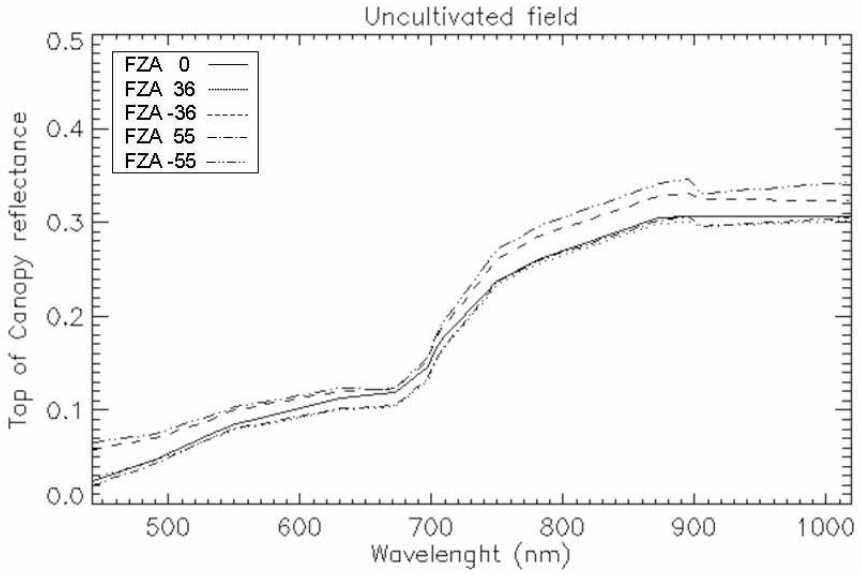

(b)

Figure 4.4: (a) multi-angular reflectance for dense forest, (b) multi-angular reflectance for uncultivated areas

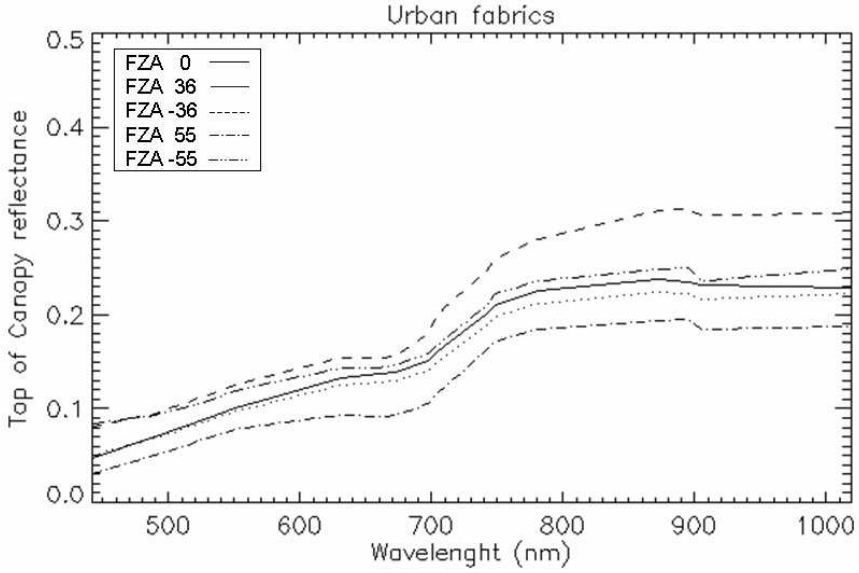

(a)

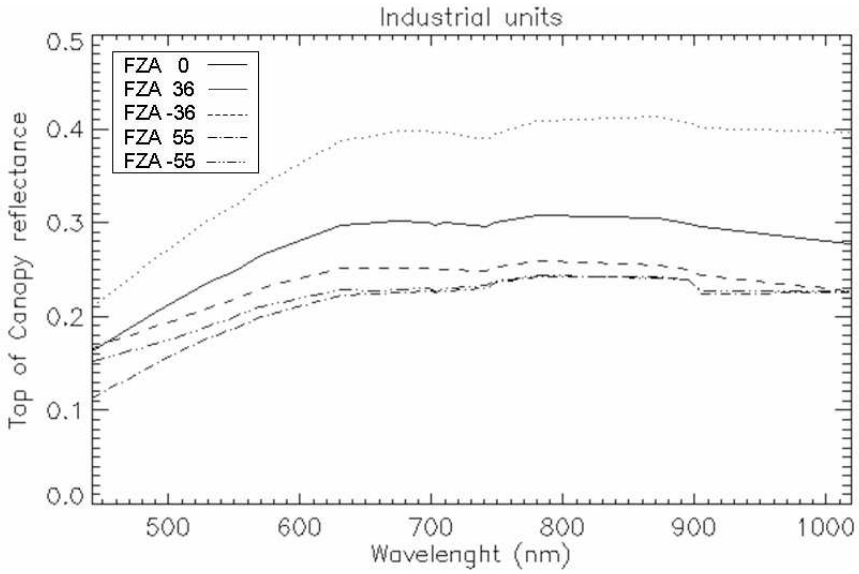

(b)

Figure 4.5: (a) multi-angular reflectance for urban residential buildings, (b) multi-angular reflectance for industrial and commercial units

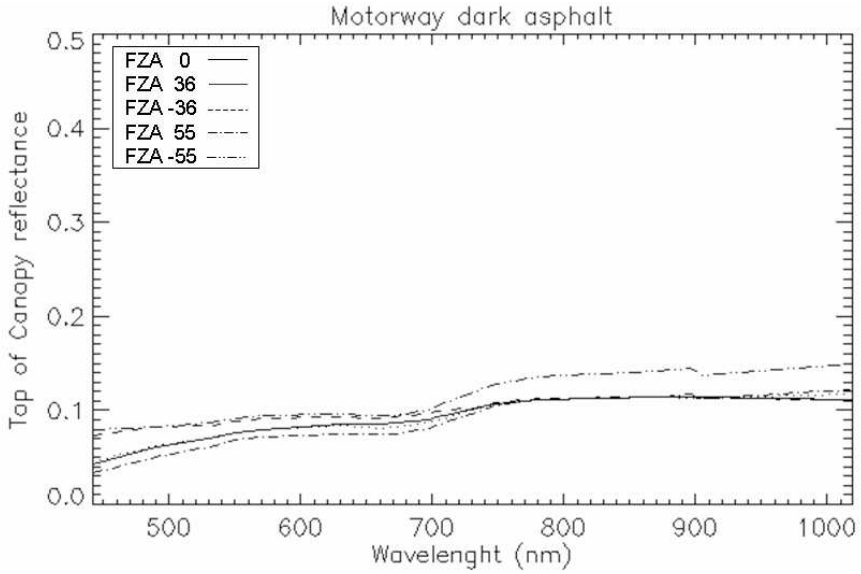

(a)

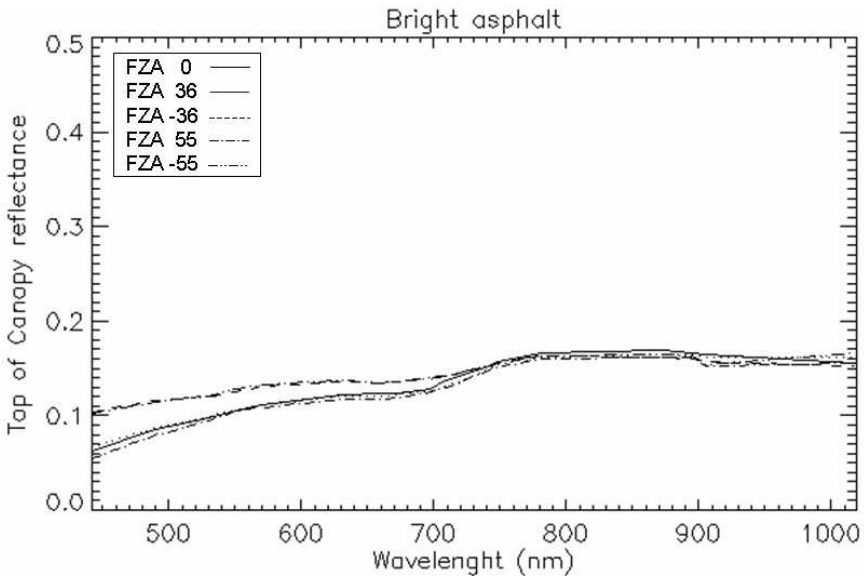

(b)

Figure 4.6: (a) multi-angular reflectance dark asphalted surface, (b) multi-angular reflectance for bright asphalted surfaces

4.3 The neural networks classification

For the decision task a pixel based classification scheme based on neural networks has been developed [22]. During the last years this kind of methodology has demonstrated at the same time a particular ease on managing a large domain of inputs and an important effectiveness in performing the decision task for the classification of remotely sensed images [23]. For each classification exercise, reported on the following sections, this approach has been proposed considering different configurations of inputs and different target classes individuated in the image. Regarding the network topology, the multi-layer perceptron (MLP) seems to be the best configuration to solve problems of classification and inversion [24] and it has been considered for this study. The learning process has been carried out using two data sets: a training set and a validation set. A third set of point has been as well collected for the validation of the final results. The number of hidden layers, and the amount of units composing each layer, have been obtained after a systematic analysis. The best configuration is found when the minimum of the error function is reached on the test set. In our applications the error function calculates the sum of squared errors (SSE) considering all patterns and it is expressed by the formula:

$$SSE = \sum_{n=1}^{N} \sum_{k=1}^{c} \{y_k(x^n; w) - t_k^n\} \tag{4.1}$$

where $y_k(x^n; w)$ represents the output of unit k as a function of the input vector x^n and the weight vector w, N is the number of testing patterns, and c is the number of outputs. The quantity t_k^n represents the target value for output unit k when the input vector is x^n. In general, for the considered cases, the number of hidden layers has been two, while the number of hidden

units changed according to the classification problem. The minimization of the error function has been pursued by a scaled conjugate gradient (SCG) algorithm, which uses the second order of derivative of the error function [25]. The Stuttgart neural network simulator (SNNS), made available by the University of Stuttgart, Germany, has been used to design the network topology and perform the learning phase.

Several test have demonstrated that the input rescaling could provide better results during the classification phases. The neural network ingests pixel values comprised between -1 and 1 while the images have values of reflectance between 0 and 1. The neural classifier can as well process this kind of image but the linear rescaling between -1 and 1 has permitted to "decompress" the spectral information in a more wide range of values, allowing a better discrimination of similar signatures.

After the neural network training phase, the classification has been obtained through the use of an IDL software properly developed for these applications, which can ingest the CHRIS images in different configurations of spectral bands, angular images and acquisition dates and it produces the final thematic maps.

4.4 Classification of hyperspectral CHRIS nadir imagery

In the first classification exercise the input vector feeding the network contained only the nadir reflectance measurements. The example reported in this part is related to the CHRIS observation of 28th February 2006 over the test site. At this stage, we identified some basic classes usually considered for the generation of land cover products from satellite high resolution

images, such as residential buildings, industrial and commercial units, bare natural soils, vegetated areas and forest (including permanent crops). Water surfaces were not present in the area but, as a distinction between two different asphalt coverages is in principle possible for different spectral signatures due to different types of materials used for the pavement, the dark asphalted and the bright asphalted classes have been added to the more traditional ones. For the same reason two urban classes have been individuated inside the macro class urban areas. The class urban buildings regards principally houses and small residential flats which present a different spectral signature with respect to the big industrial and commercial units as well as a different sensitivity to the acquisition angle.

A total number of 915 and 896 pixels have been chosen for generating the sets with the training and the test patterns, respectively. The best topology obtained for the network is characterized by 18 inputs, two hidden layers of 14 units and 7 unit of outputs. The trend of SSE values vs. the number of units in a two hidden layer topology is plotted in Fig. 4.7 and it shows that suitable network topologies can be obtained with a minimum number of 12 units per hidden layer. This error trend recurs for many neural networks trainings performed considering also others scenarios but with the same classes as output. In general the neural networks used for the classification of nadir images in these type of classes have a minimum number of 12 units per hidden layer without exceeding 16 units. The analogous analysis carried out with one hidden layer provided slightly worse results.

The classified map composed by almost 85000 pixels and obtained with the selected topology is presented in Fig. 4.8, where as the accuracy is reported in Tab. 4.1. The accuracy has been calculated selecting a significant number (5216) of ground truth points validated on VHR Quickbird imagery and by

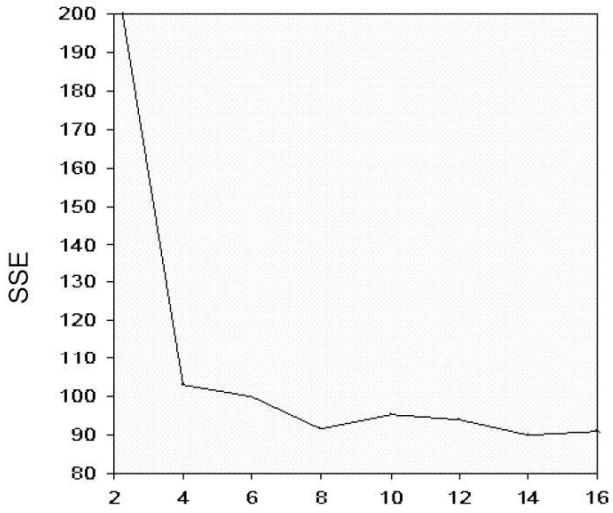

Figure 4.7: SSE vs. the number of units for hidden layers

direct inspections on site. The confusion matrix reports an overall precision of 85,7%. The result is negatively conditioned by a rather coarse performance for the bright asphalted surfaces. In fact, this feature in the images sometime appears easily confused with the adjacent pixels and with the class of urban buildings, especially when the acquisition is done under particular geometric configurations (large off-nadir angle). From Tab. 3 we note that another source of error is the confusion between bare soil and residential buildings. This is a known problem in the classification of optical images characterized by high and very high spatial resolution and is due to resemblances in the spectra between the two surfaces.

(a)

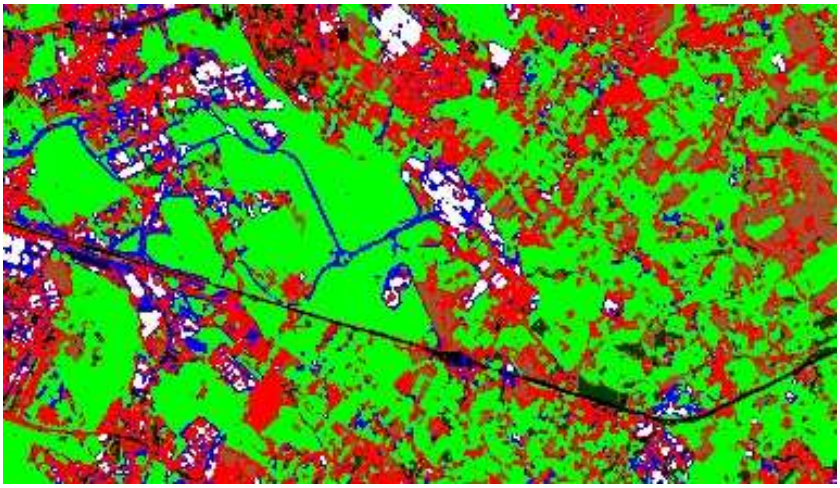

(b)

Figure 4.8: (a) Image over Tor Vergata Campus extracted from the acquisition of 28th February 2006, (b) clssified map in seven classes: dark asphalt, bright asphalt, urban buildings, industrial/commercial units (withe), bare soil, green vegetated areas, forest and permanent crops

	GROUND TRUTH						
	Dark Asphalt	Bright Asphalt	Urban Buildings	Industrial Commercial Units	Bare Soil	Green Vegetated Areas	Forest and Permanent Crops
Dark Asphalt	85.4	4.6	1.0	0.0	0.2	0.0	0.0
Bright Asphalt	0.3	53.8	6.4	1.5	0.0	0.1	0.0
Urban Buildings	10.1	27.0	84.0	1.5	29.5	0.0	0.0
Industrial Commercial Units	0.0	14.3	0.7	97.0	0.0	0.0	0.0
Bare Soil	2.1	0.3	6.1	0.0	79.1	1.9	7.3
Green Vegetated Areas	0.0	0.0	1.8	0.0	0.1	98.0	9.1
Forest and Permanent Crops	2.1	0.0	0.0	0.0	0.1	0.0	83.6

Table 4.1: Confusion matrix related to the classification of the 28th February 2006 FZA0

4.5 Classification of hyperspectral multi-angular CHRIS imagery

In the second exercise we generated the same land cover maps this time using multi-angular images as inputs. Following what is shown in the multi-angle analysis, the particular directional sensitivity of the reflectance of some surfaces produced a significant classification improvement compared to the results reported in Tab. 4.1. The acquisition is again that of 28th February 2006 over the Frascati and Tor Vergata test site, but in this case the images at FZA 36 and FZA -36 have also been considered as well as the nadir image FZA 0 for the generation of the input vector. The same sub-images as in the previous case have been extracted and after the radiometric and atmospheric corrections they have been co-registered and stacked in order to obtain a unique image composed of 54 spectral bands. The neural network has been learnt using the same training and validation datasets as the previous exercise, having in this case the best topology composed by 54 inputs, two hidden layers of 24 units and the same 7 classes of output. The land cover map is reported in Fig. 4.9. The accuracy is calculated using the same ground truth as the first classification and Tab. 4.2 shows the changes in terms of class accuracy. We can see that for residential small buildings, bare soils and asphalted surfaces a significant increase in the accuracy values has been obtained thanks to the multi-angular characterization. The overall improvement calculated for this scenario is around 7%. Considering the strong angular and directional dependence of the reflectance for industrial and commercial units, changes in accuracy could also be expected for this class, but after the classification there is no evidence of improvements. This might have happened because deformations on buildings shape are present

in the off-nadir views and for this reason an imperfect overlap of these structures could occur among the stacked images. The problematic co-registration of these pixels could generate a noise that prevented us from obtaining the expected improvement for this class. In general this problem is particularly evident for features and areas of interest characterized by few pixels. In fact in these cases, the errors introduced by several steps of co-registration and the distortions produced by a multi-directional view can reduce and sometime decrease the accuracy obtained by the use of a multi-angle dataset. We can consider for example the classifications in Fig. 4.10. The white arrow indicates an area of bare soil, which is an agricultural area maintained free from natural grass in this acquisition date. It has not been properly classified using only the spectral information provided by the nadir image. On the other hand, the classification performed having as input the multi-angular stack has produced a reasonable result, demonstrating a better performance for this target. Residential units present in this area are composed by buildings of few pixel size crossed by streets of one pixel size but clearly visible in the CHRIS image (for example the residential unit closest to the misclassified areas in Fig. 4.10). In this case classification using the nadir image has well identified the bright asphalt among the buildings and the biggest building have been reasonably classified like commercial/industrial units, but in the map obtained starting from the multi-angular stack these features have been not identified and they are replaced by the macro class residential buildings. For sure the additional information can support the automatic processing to better discriminate classes often confused because spectrally similar (typically urban and bare soil, some crops,...), but then features composed by only few pixels can be easily confused by the reason of errors due to co-registration phases and distortions related to acquisitions under very large angle of view.

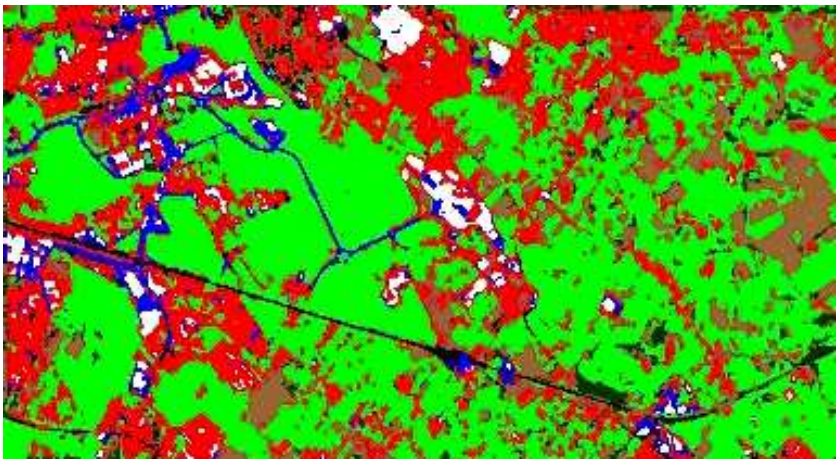

Figure 4.9: Multi-angular classification related to 28th February 2006

Surface	Imporvements
Dark Asphalt	-3%
Bright Asphalt	+27%
Urban Buildings	+10%
Industrial/Commercial Units	Not Relevant
Bare Soil	+19%
Green Vegetated Areas	Not relevant
Forest and permanent Crops	Not Relevant

Table 4.2: Improvement for the classification phase reached by the use of multi-angle information

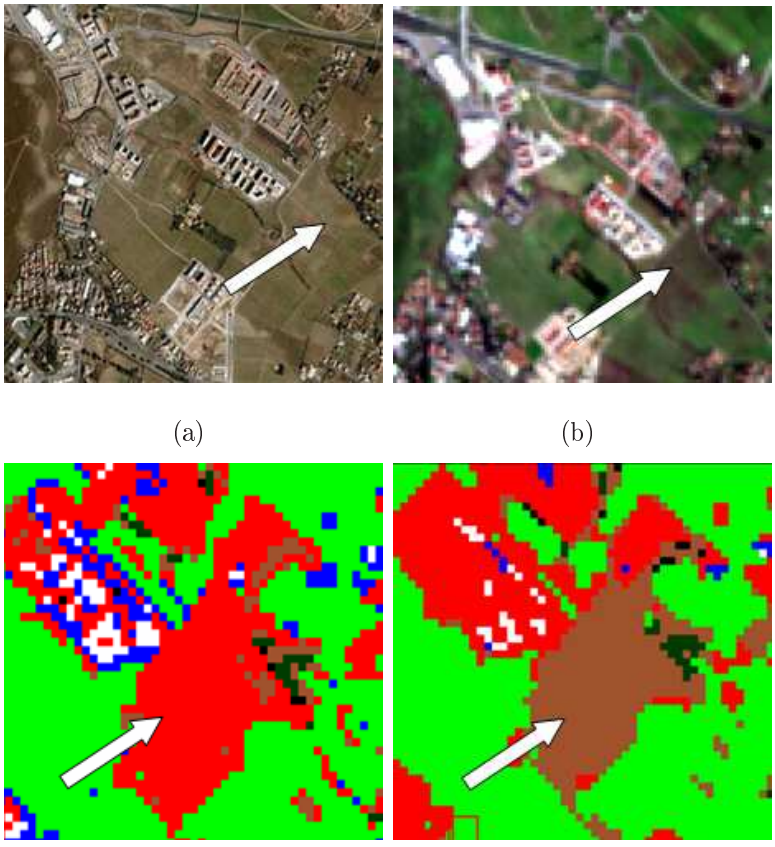

(a) (b)

(c) (d)

Figure 4.10: (a) VHR images of the commercial and residential area near Tor Vergata campus, (b) the same area acquired by CHRIS, (c) classification using the nadir image of 28th February 2006, multi-angular classification of the same acquisition

4.6 Further potentiality given by the merging of multi-temporal and multi-angular images

The PROBA mission acquisition plan allows to take more images during the same year over the same test site. This is another important characteristic of the mission which therefore allows to exploit concurrently hyperspectral, multi-angular and multi-temporal information. To analyze what is the impact of such capabilities in terms of final land cover products we performed two final classification exercises. In the first one the land cover map is obtained only with multi-temporal and multi-spectral acquisitions, in a second one the multi-angular information is added and, as in the previous section, the improvements in terms of classification accuracy evaluated.

The attempt of considering at the same time multi-angular and multi-temporal acquisitions led to a redefinition of the area of interest, even if belonging to the same test site. This is due to different concurrent reasons such as sensible shifts affecting the images acquired at different times, shifts between images taken at different angles, sensitivity to clouds, need of limiting the co-registration errors. Because of the same kind of constraints we also had to restrict the multi-angular information to 2 different angles (FZA 0, FZA 36) related to only one acquisition.

The multi-temporal information is based on three images taken at the following dates: February the 28th, August the 19th and October the 9th 2006 Fig. 4.11. These dates are chosen to minimize the difficulties listed before, but in any case they are in principle particularly suitable to monitor some important stages of crops growth cycle. The acquisition at the end of winter is particularly useful to observe the ploughing phase for the agricultural fields and in particular for the corn fields that during this time are arranged

(a)

(b)

(c)

Figure 4.11: (a) acquisition of October the 28th, (b) acquisition of August the 19th and (c) acquisition of October the 9th

for the next seed in April. In August most of the crops present in this area are going to have their maximum of the photosynthetic phase as for example vineyards, corn and other crops while not currently used natural areas are covered by dry grass or sparse vegetation and they are characterized by a lower reflectance in the infrared range. Finally, the acquisition of October is used to monitor cereals, crops and vineyards harvested in this period as well as agricultural field ploughed in this period to be ready for the winter cultivations. The reflectance seems to follow all these phases and significant changes are observed during the development phases. For example in in Fig. 4.12 we report two examples which show how cultivated areas, such as corn fields or vineyards, change significantly their spectra during the year. However, the vegetation development is peculiar for each particular crop type, provoking significant differences in the associated multi-temporal signatures. Therefore positive effects particularly on crops discrimination can be expected. With respect to the previous cases the vineyards and corns fields, largely diffused in the selected area, have been extracted from the permanent crops class and vegetated areas class, respectively, and considered as separated classes. We also treated uncultivated areas as a single class. In fact, their dependence with time should be rather different from that of cultivated fields. On the other side we eliminated the bare soil class, as most of bare soils are cultivated fields at the very beginning of the growth cycle or after the harvest. Summarizing we had to discriminate among 9 classes with an input vector including 54 measurements (3 images of 18 bands).

A new neural network algorithm has been trained using a training set and a test set of 3120 and 3045 patterns, respectively. A third different set of 21766 ground-truth pixels has then been considered for the computation of the confusion matrix reported in Tab 4.3, while the classification and map is

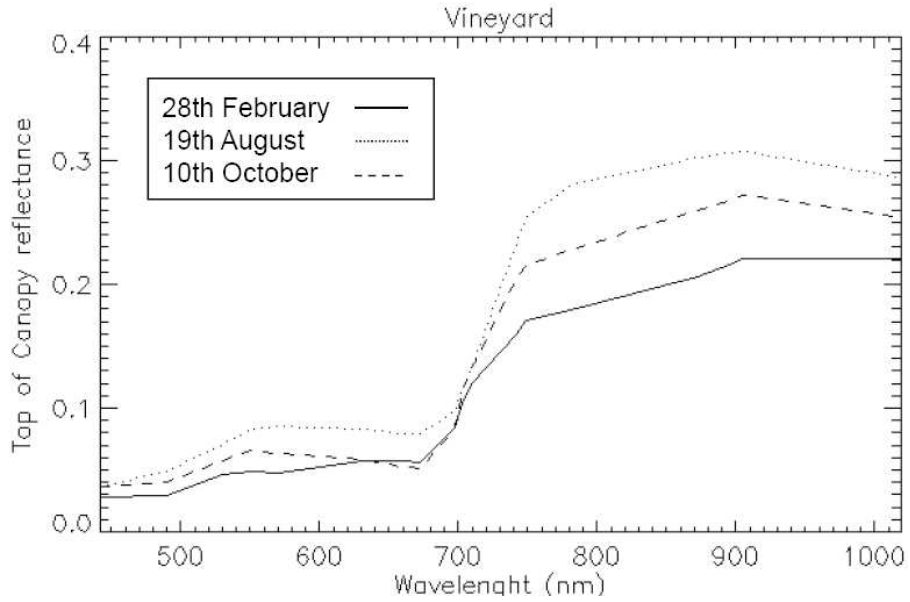

(a)

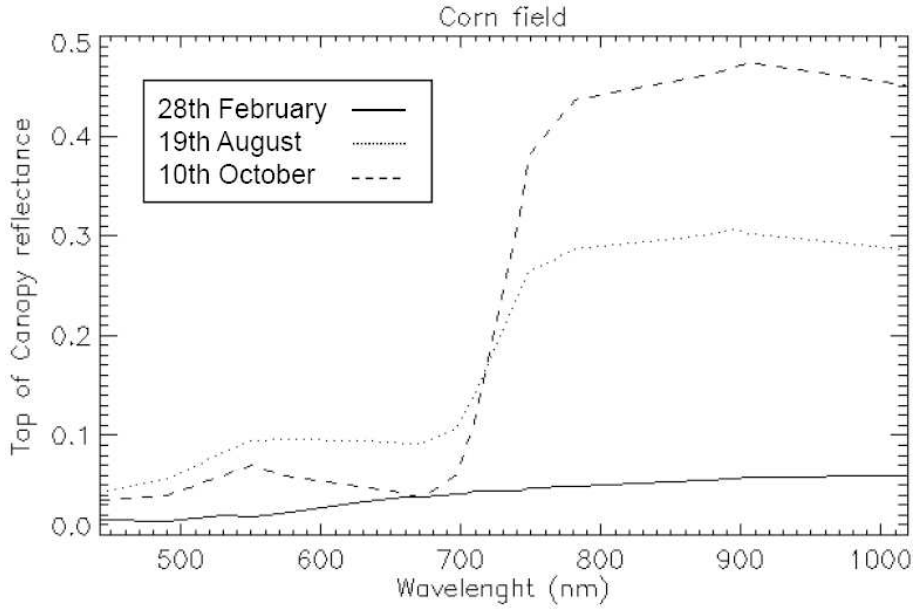

(b)

Figure 4.12: (a) multi-temporal reflectance for vineyards, (b) multi-temporal reflectance for corn fields

shown in Fig. 4.13

The same procedure has been applied to a new network having in input also multi-angular information. The acquisition at the FZA 36° of the second date (month of August) was the additional piece of information. The choice of this date stems from the fact that the multi-angular information should carry the best contribution when the agricultural fields are at the stage of full development. The corresponding results are reported in and Fig. 4.13 and Tab. 4.4. The validation on the ground-truth demonstrates that both classifications have reported an high accuracy over all classes, always above 87 for any single class if we considered vineyards and other permanent crops as a unique class, with an overall improvement on the performance of more than 5 when the combined temporal and angular information is provided to the network. In particular, the most significant increase in the accuracy has been obtained for dark asphalted surfaces, uncultivated areas and vineyards. The class of vineyard shows the best improvement, 11%, definitely mitigating the confusion with other permanent crops (olive-groves and orchards). We do not have a better accuracy in all classes though. For the bright asphalt it decreases of 2%, probably due to the errors introduced by a further step of co-registration.

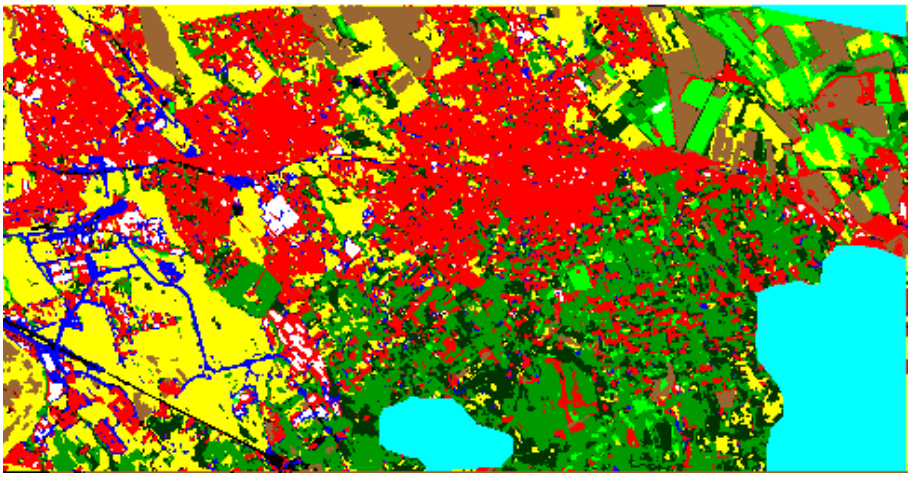

(a)

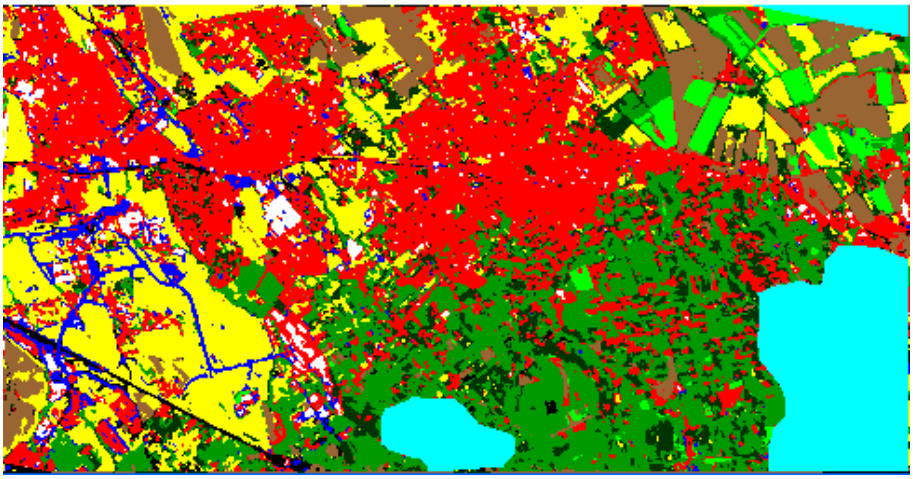

(b)

Figure 4.13: (a) multi-temporal classification, (b) multi-temporal and multi-angular classification.Dark asphalt, bright asphalt, urban buildings, industrial/commercial units (withe), uncultivated, Others permanent crops, Vineyards, Corn, Others agricultural areas, masked areas (clouds and shadows)

	GROUND TRUTH								
	Dark Asphalt	Bright Asphalt	Urban Buildings	Industrial Commercial Units	Uncultivated	Others Permanent Crops	Vineyards	Corn	Others agricultural areas
Dark Asphalt	88.73	1.41	0.04	0.44	0.04	0.00	0.06	0.00	0.00
Bright Asphalt	1.41	92.94	0.92	0.66	0.23	0.00	0.02	0.00	0.00
Urban Buildings	4.93	4.00	96.21	4.18	0.27	0.00	2.31	0.16	4.78
Industrial Commercial Units	0.00	1.41	2.20	94.73	0.00	0.00	0.00	2.02	0.00
Uncultivated	4.93	0.24	0.35	0.00	86.41	1.71	5.10	0.08	0.00
Others Permanent Crops	0.00	0.00	0.13	0.00	3.32	82.91	15.70	0.00	0.00
Vineyards	0.00	0.00	0.15	0.00	5.67	14.1	73.02	2.58	0.55
Corn	0.00	0.00	0.00	0.00	3.57	0.21	3.54	95.16	0.10
Others agricultural areas	0.00	0.00	0.00	0.00	0.49	1.07	0.26	0.00	94.56

Table 4.3: Confusion matrix for the multi-temporal classification (3 dates) of the nadir images. The reported values are in %

SURFACE	IMPROVEMENTS
Dark Asphalt	+6%
Bright Asphalt	-2%
Urban Buildings	Not Relevant
Industrial Commercial Units	Not Relevant
Uncultivated	+8%
Others Permanent Crops	+1%
Vineyards	+11%
Corn	+2%
Others Agricultural Areas	+4%

Table 4.4: Improvements obtained with the use of multi-angle and multi-temporal acquisitions

4.7 Comparison between ETM+ and CHRIS

This last exercise proposes a comparison between ETM+ Landsat and CHRIS Proba images in terms of classification accuracy. Since years, ETM+ has been the most used optical multi-spectral instruments for land cover, while the new spectral configuration of CHRIS has been only recently introduced. The spectral differences have been already outlined on the first chapter (Fig. 2.4). In general, differences in surfaces discrimination are expected, but in this section the classes mostly influenced will be better individuated and analyzed.

Considering the images available for this work (Chapter 1), it has not been possible to compare images obtained by simultaneous acquisitions (same day, same year, same time) and for this reason this investigation has been done selecting images which have been acquired with a short time delay. The best configuration which has been found takes into account an ETM+ acquisition of 19 August 2004 and a CHRIS Proba image of 19 August 2006 Fig. 4.14. Despite the two images are separated by two years, the day of acquisition is the same and it is possible to assume same conditions of illumination and same photosynthetic state for crops and vegetated areas. The others two ETM+ images, acquired during the 2001, have not been actually considered because many land cover changes have been observed, especially in agricultural areas, vineyards and urban buildings [26]. The different spatial resolution of the two product has been compensated by a further resempling step, which has decreased the CHRIS resolution from 21m to 32m, making possible a satisfactory overlap of features, structures and areas present on both images. This has permitted to select the same areas for the neural network training (training and test sets) and for the final validation. The same nine classes of land cover have been individuated inside this scenario:

(a)

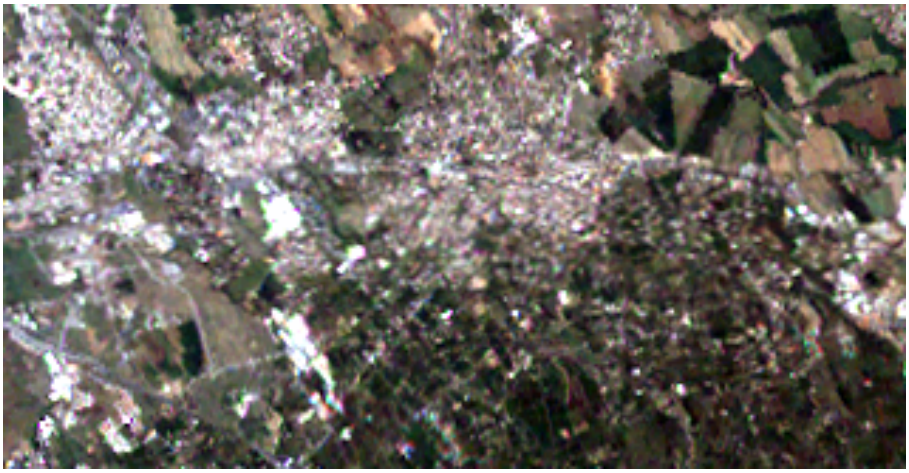

(b)

Figure 4.14: (a) CHRIS acquisition of 19th 2006, (b) ETM+ acquisition of 19th August 2004

dark asphalt, bright asphalt, urban buildings, industrial/commercial units, corn fields, vineyards, other permanent crops like olive and fruit trees, uncultivated vegetated areas, bare soils. The neural network training phase has produced two different topologies with the minimum error calculated considering the test set. For the the ETM+ the best configuration consists on a network of 6 inputs, two layers of 14 units each and 9 outputs, while for

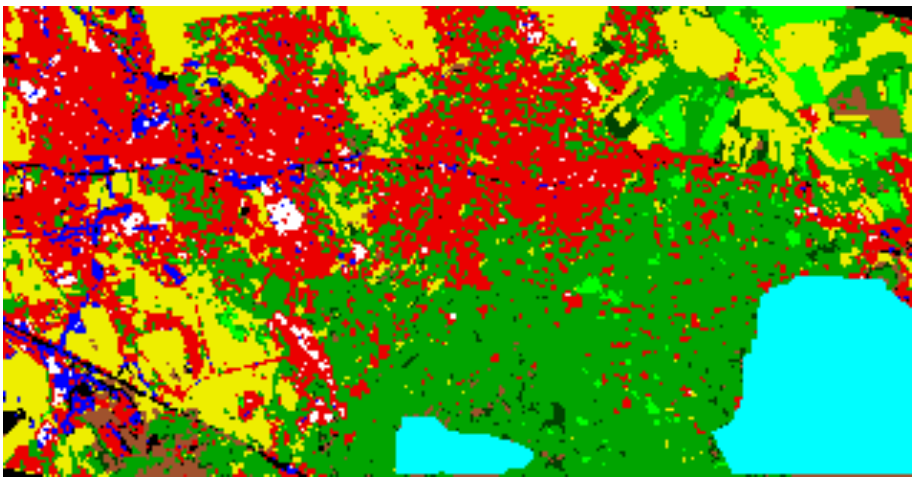

(a)

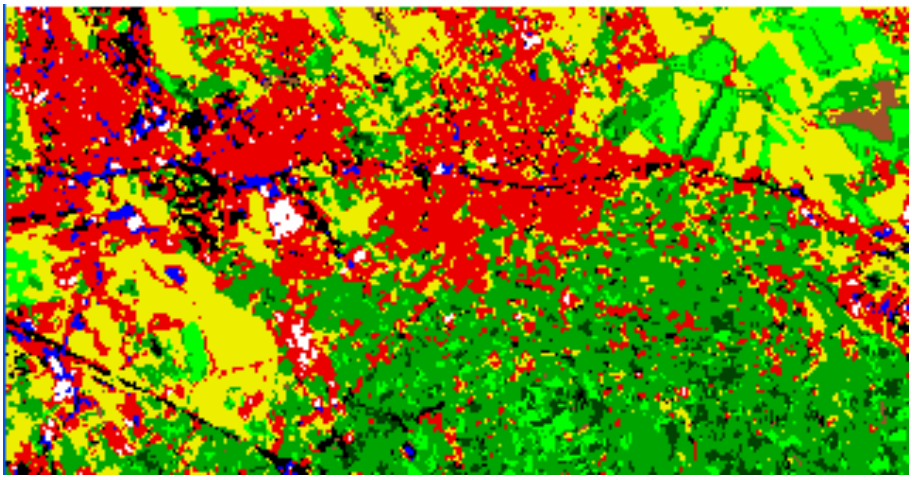

(b)

Figure 4.15: (a) classification related to CHRIS acquisition of 19th 2006, (b) classification related to ETM+ acquisition of 19th August 2004.

the CHRIS it consists on 18 inputs, two layers of 16 inputs and 9 outputs. The maps generated are reported in Fig. 4.15 The two classification exercises, related to this scenario and to this acquisition date, have provided overall accuracies respectively of 75.65% for ETM+ and 79.85% for CHRIS considering an overall number of validation pixel equal to 10.500. These low accuracies are strongly conditionated by low performances for classes like asphalts (dark

SURFACE	CHRIS IMPROVEMENTS
Dark Asphalt	+13%
Bright Asphalt	+25%
Urban Buildings	+6%
Industrial Commercial Units	+15%
Uncultivated	-5%
Bore Soil	+15%
Others Permanent Crops	+12%
Vineyards	+12%
Corn	+10%

Table 4.5: Improvements obtained using the CHRIS product with respect to ETM+ image

and bright), which are difficult to discriminate at this coarser resolution and by classes such as vineyard, uncultivated and permanent crops, which are not easy to differentiate with only one acquisition. In any case a mean improvement of 4% results using the CHRIS spectral configuration and considering the overall pixels. But considering each class separately, the improvements could change how reported in Tab. 4.5 Starting with the artificial surfaces, the improvements for the two types of asphalt and for the industrial units are relevant, while for the urban buildings the improvement is around the 6%. In particular, the bright asphalt is better identified and separated from the others man-made surfaces, reporting at the end the best improvement of +25%. If we consider the agricultural areas as a unique class, CHRIS and ETM+ demonstrate similar performances, but analyzing each class separately, CHRIS demonstrates a better capability in crops discrimination and in particular the vineyards and the permanent crops are better identified

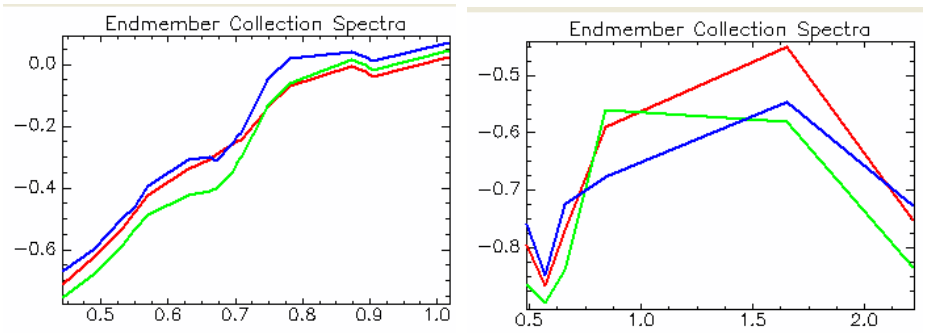

(a) (b)

Figure 4.16: Signature extracted for urban buildings, vineyard, uncultivated: (a) CHRIS signature, (b) ETM+ signature. The values represents reflectances resclated between -1 and 1

reporting an improvement of +12%. In fact ETM+ tends to confuse this class with corn and others permanent crops like olive and fruit trees. For the natural areas, represented in this exercise by bare soil and uncultivated zones, improvements have been observed only for the first class while for the uncultivated areas ETM+ has provided better results in several cases. In fact, considering the classification related to the CHRIS image, many uncultivated field have been wrongly classified like urban and vineyards. The spectral analysis, which has been performed over some of these misclassified areas, has reported for CHRIS an objective spectral similarity for these three signatures. On the other hand, the spectral plots extracted form the ETM+ image seems to have very different trends and values in some spectral ranges. The Fig. 4.16 shows an example of signatures extracted from a misclassified area close to the Casilina state street Fig. 4.17. The CHIRS signatures are very similar and overlapped in some bands while the ETM+ signatures present spectral differences for bands around 1,6 μ and 2.2 μ, which are not present in CHRIS. This similarity for the CHRIS signatures has produces a series of ambiguities for the uncultivated class during the classification phase,

but the same have been mitigated in the ETM+ classification by the presence of bands located in the Short Wave Infrared (SWIR).

(a)

(b) (c)

Figure 4.17: (a) VHR image over one area not correctly classified in the CHRIS classification, (b) CHRIS image, (c) ETM+ image

Chapter 5

Conclusions

In this research work we have investigated the potential of CHRIS imagery to automatically produce maps of land cover, considering as test site the area of Frascati and Tor Vergata. The use of this kind of images could be well considered an innovation for the classification of optical satellite data, especially if we consider the new spectral configuration and the new acquisition capability introduced with this mission. The developing of preprocessing steps, methodologies and software tools has been necessary in order to design optimum classifying schemes. This complete treatment of CHRIS imagery for "end to end" applications can be considered a first significant result of this work. Problems like the correction of radiometric artifact, the compensation of the atmospheric contributions and the ortho-rectification have been faced proposing satisfactory and improved solutions. In particular the correction of stripes, present along the columns direction, has required a deep review of methodologies already available for others missions, which have been tested for the CHRIS products. Finally, a semi-automatic tools for the destriping based on the low-pass filtering in the spatial frequency domain has been developed and tested. This methodology has permitted to correct these artifacts

without affecting the radiometric and geometric quality of the image. Satisfactory results have been obtained for different scenarios, and the impact of "noisy" areas such as clouds, shadows, boundaries of heterogeneous surfaces, has been reduced and in some cases deleted. The atmospheric correction has been done simulating the radiative quantities (solar irradiance at bottom of atmosphere, transmittance of the path and aerosols scattering) through the use of a radiative transfer model. The model takes as inputs many parameters which have been integrated with on site measurements with the principal purpose of better estimates seasonal and daily trends concerning the aerosols and the water vapor content. Finally the images of reflectance have been obtained.

The second aspect of the study deals with the new capabilities offered by the Proba mission and CHRIS imagery in terms of information retrieval. The platform is conceived to monitor a region of interest at high spatial resolution (around 20m) with hyperspectral, multi-angular and multi-temporal measurements. The possibility of integrating these three types of information for the decision task gives to the CHRIS image dataset an exceptionality potential. The classification exercises performed during this research work have tried to asses the real impact of joined spectral, directional and temporal information for the identification of different land cover types. The classification performed using only the nadir image has permitted to discriminate with a satisfactory accuracy (more than 80%) 6 classes of land cover, including two different types of asphalts and urban fabrics. The inclusion in the input vector of the spectra corresponding to 3 angular acquisitions (FZA at namely -36°, 0° and +36°) has been important to mitigate some misclassified areas still present in the map obtained by the nadir image. In particular structures related to the urban classes like roads, buildings, asphalted areas,

have received the best improvements and also the typical ambiguity between urban and some kinds of bare soils have been satisfactory resolved. The overall classification accuracy reached in the multi-temporal classification results more than 92%, an improvement of almost 7% with respect to single nadir acquisition has been obtained. We have also seen that a further increase of the classification quality may derive from the consideration in the processing scheme of the multi-temporal measurements. We observed that the information brought in by multi-temporal data, besides refining the classification in terms of discrimination levels, can also improve the accuracy rates, leading to overall accuracies of about 93% considering 9 different classes.

Once again our study demonstrates the effectiveness of neural network algorithms in positively combining different levels of information. Moreover the good suitability of the MLP neural network for problems of decision and classification has been confirmed and verified also in this case. In particular, topologies characterized by two hidden layers with a minimum number of 12 hidden units have provided good results for all the exercises previously proposed. The principal disadvantage of this kind of approach could regard the dimension of the input vector. In fact especially when more multi-temporal and multi-directional acquisitions will be available during one year and over the same test site, we may easily reach hundreds of components for the input vector of the classification algorithm. Until now no particular problems of computational power have been encountered, but for sure the increasing number of inputs can make difficult the neural network training and classification. At this point a selection of the inputs as well as the pruning of the network will be unavoidable to eliminate unnecessary or misleading quantities and it could be considered the logic continuity and improvements for this work.

Bibliography

[1] D.J. Diner, Beckert J.C., Reilly T.H., Bruegge C.J., Conel J.E., Kahn, R.A., Martonchik J.V., Ackerman T.P., Davies R., Gerstl S.A.W., Gordon H.R., Muller J.-P., Myneni R.B., Sellers P.J., Pinty B., Verstraete M.M.,"Multi-angle Imaging SpectroRadiometer (MISR) instrument descriptionand experiment overview", *IEEE Transactions on Geoscience and Remote Sensing*, VOL: 36, No. 4, pp. 1072-1087, July 1998

[2] V. N. Sridhar, R. R. Navalgund, Mahtab, A., "Impact of Surface Anisotropy on Classification Accuracy of Selected Vegetation Classes: An Evaluation Using Multidate Multiangular MISR Data Over Parts of Madhya Pradesh, India", *IEEE Transactions on Geoscience and Remote Sensing*, Vol. 46, No. 1, pp. 250-258, January

[3] S. Mukai and I. Sano, "Retrieval algorithm for atmospheric aerosols based on multi-angle viewing of ADEOS/POLDER", *Earth Planets Space*

[4] M. Berger, M. Rast, P. Wursteisen, E. Attema, J. Moreno, A. Müller, U. Beisl, R. Richter, M. Schaepman, G. Strub, M.P. Stoll, F. Nerry, M. Leroy, "The DAISEX Campaigns in Support of a Future Land-Surface-Processes Mission", *ESA bulletin*, No. 105 , February 2001

[5] W. Huang; Niu, Z.; Wang, J.; Liu, L.; Zhao, C.; Liu, Q., "Identifying Crop Leaf Angle Distribution Based on Two-Temporal and Bidirectional Canopy Reflectance", *IEEE Transactions on Geoscience and Remote Sensing*, Vol 44, No. 12, pp. 3601-3609, December 2006

[6] Michael J. Barnsley, Jeff J. Settle, Mike A. Cutter, Dan R. Lobb, and Frederic Teston, "The PROBA/CHRIS Mission: A Low-Cost Smallsat for Hyperspectral Multiangle Observations of the Earth Surface and Atmosphere", *IEEE Transaction on Geoscience and Remote Sensing*, Vol. 42, no. 7, July 2004

[7] M.Cutter, *CHRIS Data Format*, issue 4.2

[8] M.Davidson, *Note on CHRIS acquisitions procedure and image geometry*, issue 1

[9] B.K.P. Horn and R.J. Woodham, "Destriping Landsat MMS Images by Historgroam Modification", *Computer Graphics and Image processing 19*, 69-83, 1979

[10] J. Chen, Y. Shao, H. Guo, W. Wang and B. Zhu, "Destriping CMODIS Data by Power Filtering", *IEEE Transaction on Geoscience and Remote Sensing*, Vol. 41, no. 9, September 2003

[11] J. Torres and S.O. Infante, "Wavelet analysis for the elimination of striping noise in satellite images", *Opt. Eng.*, vol. 40, no. 7, pp.1309-1314, Jul. 2001

[12] http://earth.esa.int/object/index.cfm?fobjectid=4409

[13] J.C. Garcia and J. Moreno, "Removal of noises in CHRIS/Proba images: application to the SPARC Campaign data", Proceeding of Second Chris Proba Woorkshop, ESA ESRIN, 28-30 April 2004

[14] *Télédétection et Taitement des images - Introduction*

[15] S.K. Mitra, *Digital signal processing, a computer based approach*, McGraw-Hill, Second Edition, pp.315,2001

[16] B. Mayer, A. Kylling, "Technical note: The libRadtran software pachage for radiative tranfer calculations-description and example of use", *Atmospheric Chemistry and Physics*, 5, 1855-1877,2005

[17] B. Mayer, A. Kylling, *libRadtran manual*, edition 1.0, December 2006

[18] http://aeronet.gsfc.nasa.gov

[19] E. Vermote, N. El Saleous, C. Justice, Y. Kaufman, J. Privette, L. Remer, J. Roger, D. Tanrè, "Atmospheric correction of visible to middle-infrared EOS-MODIS data over land surfaces: Bacgorungd, operational algorithm and validation", Jpurnal Of Geophysical Research, Vol. 102, No. D14, pp.17,131-11,141,1997

[20] Leica Geosistem ERDAS field Guide, 7th edition

[21] *Corinne Land Cover, Part One-Methodology*

[22] C. Bishop, *Neural Networks for Pattern Recognition*, Oxford Univ. Press, New York, 1995.

[23] F. Del Frate, F. Pacifici, G. Schiavon, C. Solimini, "Use of neural networks for automatic classification from high resolution imagery", *IEEE*

Transaction on Geoscience and Remote Sensing, Vol. 45, No. 4, April 2007

[24] S. Y. Hsu, T. Masters, M. Olson, M. Tenorio, and T. Grogan, "Comparative analysis of five neural network models", *Remote Sens. Rev.*, 6, 319-329, 1992.

[25] M. Møller, "A scaled conjugate gradient algorithm for fast supervised learning", *Neural Networks*, vol. 6, pp. 525-533, 1993.

[26] L. Fusco, E. Loret, A. Michella, J. Antunes, *Il progetto Baccus, una applicazione di tecniche avanzate per il rilevamento e la gestione di superfici vitate*, VIII Conferenza nazionale ASITA, Roma 14-17 December, 2004

Curriculum Vitae

Riccardo Duca received the Laurea (B.S.) and Laurea Specialistica (M.S.) degrees in telecommunication engineering at Tor Vergata University of Rome, in 2002 and 2004, respectively. Since October 2004 he is PhD candidate in Geoinformation at Tor Vergata University of Rome and he is visiting scientist at ESA ESRIN, Frascati (Italy). From October 2006 until May 2007 he worked in the TEC-EEP section at ESA ESTEC, Noordwijk (The Netherlands), contributing to the preparation of the future multi-spectral mission Sentinel-2. During his career he has been also involved in many others projects regarding the processing and the exploitation of microwave and optical remotely sensed images and their integration in Geographic Information Systems.

His main research activity regards the processing and the use of multi-spectral and hyperspectral high resolution imagery for targets and surfaces identification. In particular, most of his work has been addressed towards the evaluation of the space and airborne hyperspectral technology for the generation of land cover maps and for the simulation of future multi-spectral instruments.

Conferences, Publications and Seminars

Conferences:

- R. Duca, F. Del Frate, F. Parmiggiani, "Monitoring of Terra Nova Bay Polynya with ASAR Wide Swath images", ENVISAT Symposium 2004, Salzburg
- R. Duca, F. Del Frate, "Hyperspectral CHRIS Proba imagery over the area of Frascati and Tor Vergata: rerecent advances on radiometric correction and atmospheric calibration", 4th CHRIS Proba Workshop, ESA ESIRN Frascati (Italy), 19 September 2006
- F. Del Frate, R. Duca, D. Solimini, "Urban features retrieved by hyperspectral multi-angle CHRIS/Proba images", URBAN 2007, Paris (France), April 11-13, 2007
- F. Del Frate, R. Duca, D. Solimini, "The potential of hyperspectral and multi-angle CHRIS/Proba images in vegetation identification and monitoring", Envisat Symposium 2007, Montreux (Switzerland), April 23-27, 2007
- F. Del Frate, R. Duca, D. Solimini, "Use of CHRIS/Proba Images for

land use product" Proceeding IGARSS 2007, Barcelona (Spain), July 23-27, 2007

- F. Del Frate, R. Duca, "Feature extraction potentialities of Multi-Angle CHRIS Proba Imagery" ESA EUSC 2008, ESRIN Frascati (Rome), March 4-6, 2008

Publications

- R. Duca, F. Del Frate,"Hyperspectral and multi-angle Chris Proba Images for the generation of land cover maps", *IEEE Transaction on Geoscience and Remote Sensing*, accepted

Seminars

- R. Duca, "Hyperspectral CHRIS Proba imagery: recent advances on radiometric correction and atmospheric calibration", Tor Vergata Geoinformation Seminar, Rome, 12 May 2006

- R. Duca, F. Sarti, A. Minchella, "Tsunami (Asia) of 26/12/2004: change detection dataset of ENVISAT ASAR and MERIS, ERS1 and ERS2 SAR, CHRIS/PROBA acquisitions. Region of the Andaman and Nicobar Islands and Northern Sumatra. Preliminary Results", Final presentation after ESA dataset preparation for the Tsunami event, ESA ESRIN Frascati (Rome), June 2005

- R. Duca, "Evaluation of Sentinel-2 Image Quality as a Function of the Compression Ratio", ESA ESTEC Noordwijk (The Netherlands), 30 May 2007